# Edinburgh Research Explorer

# Air Pollution Particulate Matter Exposure and Chronic Cerebral Hypoperfusion and Measures of White Matter Injury in a Murine Model

# Research

# Air Pollution Particulate Matter Exposure and Chronic Cerebral Hypoperfusion and Measures of White Matter Injury in a Murine Model

*Qinghai Liu,[1] Kristina Shkirkova,[1] Krista Lamorie-Foote,[1] Michelle Connor,[2] Arati Patel,[3] Robin Babadjouni,[4] Mikko Huuskonen,[1,5] Axel Montagne,[1,5] Hans Baertsch,[1] Hongqiao Zhang,[9] Jiu-Chiuan Chen,[6] Wendy J. Mack,[6] Brian P. Walcott,[7] Berislav V. Zlokovic,[1,5] Constantinos Sioutas,[8] Todd E. Morgan,[9] Caleb E. Finch,[9] and William J. Mack[1,10]*

[1]Zilkha Neurogenetic Institute, University of Southern California, Los Angeles, California, USA
[2]Department of Neurosurgery, Washington University School of Medicine, St. Louis, Missouri, USA
[3]Department of Neurological Surgery, University of California San Francisco School of Medicine, San Francisco, California, USA
[4]Department of Neurological Surgery, Cedars-Sinai, Los Angeles, California, USA
[5]Department of Physiology and Neuroscience, University of Southern California, Los Angeles, California, USA
[6]Department of Preventative Medicine, University of Southern California, Keck School of Medicine, Los Angeles, California, USA
[7]Department of Neurosurgery, Northshore Neurological Institute, Evanston, Illinois, USA
[8]Department of Civil and Environmental Engineering, Viterbi School of Engineering, University of Southern California, Los Angeles, California, USA
[9]Leonard Davis School of Gerontology, University of Southern California, Los Angeles, California, USA
[10]Department of Neurological Surgery, Keck School of Medicine, University of Southern California, Los Angeles, California, USA

**BACKGROUND:** Exposure to ambient air pollution particulate matter (PM) is associated with increased risk of dementia and accelerated cognitive loss. Vascular contributions to cognitive impairment are well recognized. Chronic cerebral hypoperfusion (CCH) promotes neuroinflammation and blood–brain barrier weakening, which may augment neurotoxic effects of PM.

**OBJECTIVES:** This study examined interactions of nanoscale particulate matter (nPM; fine particulate matter with aerodynamic diameter $\leq 200\,nm$) and CCH secondary to bilateral carotid artery stenosis (BCAS) in a murine model to produce white matter injury. Based on other air pollution interactions, we predicted synergies of nPM with BCAS.

**METHODS:** nPM was collected using a particle sampler near a Los Angeles, California, freeway. Mice were exposed to 10 wk of reaerosolized nPM or filtered air (FA) for 150 h. CCH was induced by BCAS surgery. Mice (C57BL/6J males) were randomized to four exposure paradigms: *a*) FA, *b*) nPM, *c*) FA + BCAS, and *d*) nPM + BCAS. Behavioral outcomes, white matter injury, glial cell activation, inflammation, and oxidative stress were assessed.

**RESULTS:** The joint nPM + BCAS group exhibited synergistic effects on white matter injury ($2.3\times$ the additive nPM and FA + BCAS scores) with greater loss of corpus callosum volume on T2 magnetic resonance imaging (MRI) (30% smaller than FA group). Histochemical analyses suggested potential microglial-specific inflammatory responses with synergistic effects on corpus callosum C5 immunofluorescent density and whole brain nitrate concentrations ($2.1\times$ and $3.9\times$ the additive nPM and FA + BCAS effects, respectively) in the joint exposure group. Transcriptomic responses (RNA-Seq) showed greater impact of nPM + BCAS than individual additive effects, consistent with changes in proinflammatory pathways. Although nPM exposure alone did not alter working memory, the nPM + BCAS cohort demonstrated impaired working memory when compared to the FA + BCAS group.

**DISCUSSION:** Our data suggest that nPM and CCH contribute to white matter injury in a synergistic manner in a mouse model. Adverse neurological effects may be aggravated in a susceptible population exposed to air pollution. https://doi.org/10.1289/EHP8792

## Introduction

The joint effects of environmental exposures and underlying health conditions are understudied. Evidence from epidemiological and animal investigations suggest that exposure to traffic-related particulate matter (PM) less than 2.5 μm in diameter ($PM_{2.5}$) is associated with increased risk of dementia (Tsai et al. 2019; Peters et al. 2019) and recent data link air pollution exposure and neurocognitive decline (Cacciottolo et al. 2017; Kulick et al. 2020; Petkus et al. 2020; Tonne et al. 2014; Younan et al. 2020). Vascular contributions to cognitive impairment and dementia are also well-established (de la Torre 2004; Emrani et al. 2018; Sweeney et al. 2019). The hypothesis has been advanced that PM may differentially affect individuals with preexisting or concurrent neurological diseases (Block et al. 2012). This hypothesis was indirectly supported by separate lines of studies conducted in mice suggesting that PM exposure and chronic cerebral hypoperfusion (CCH) each promote pathophysiological processes that can amplify white matter neurotoxicity resulting from the other (Babadjouni et al. 2018; Liu et al. 2013, 2019). However, this important hypothesis has not been directly tested in appropriate study populations or experimental models.

Recent epidemiological and experimental investigations have demonstrated PM effects on myelin tracts and white matter structures. $PM_{2.5}$ exposures were associated with decreased regional white matter volumes in the corpus callosum and frontal/temporal lobes of community-dwelling older women (Chen et al. 2015) and total white matter volumes in the general population (Erickson et al. 2020). Experimental data demonstrated myelin changes in the hippocampal CA1 region following rodent ultrafine PM exposures (Woodward et al. 2017b). Accumulating laboratory evidence suggested that traffic-related air pollution results in neuroinflammation and oxidative stress in multiple brain regions (Bos et al. 2012; Campbell et al. 2005; Morgan et al. 2011). Specifically, regional complement C5 deposition and microglial activation were demonstrated in the corpus callosum

**Note to readers with disabilities:** *EHP* strives to ensure that all journal content is accessible to all readers. However, some figures and Supplemental Material published in *EHP* articles may not conform to 508 standards due to the complexity of the information being presented. If you need assistance accessing journal content, please contact ehponline@niehs.nih.gov. Our staff will work with you to assess and meet your accessibility needs within 3 working days.

of mice following 10-wk ultrafine PM exposures (Babadjouni et al. 2018).

Cerebral hypoperfusion was associated with both neurodegeneration (Benedictus et al. 2014) and dementia (Wolters et al. 2017). Radiographic investigations have shown evidence of cerebral hypoperfusion in patients with Alzheimer's disease (AD) and in those with mild cognitive injury. Reduced cerebral blood flow was associated with increased white matter hyperintensity burden in older adults (Crane et al. 2015; van Dalen et al. 2016). A recent investigation demonstrated correlations between reduced cerebral blood flow and white matter volumes in patients with neuropsychologically defined mild cognitive impairment. Lobar region of interest-based linear regression showed significant associations between white matter lesion volume and mean cerebral blood flow in the parietal ($t_{(15)} = -3.00$, $p = 0.009$), temporal ($t_{(15)} = -3.89$, $p = 0.001$), and occipital lobes ($t_{(15)} = -4.71$, $p < 0.001$) (Kim et al. 2020). Lesion volumes in this study appeared more consistent with white matter hyperintensities rather than the normal appearing/total white matter volumes that epidemiological reports have demonstrated as having associations with air pollution. CCH increased blood–brain barrier (BBB) permeability and upregulated inflammatory mediators in rodent models (Choi et al. 2016; Liu et al. 2019). These alterations can increase penetration and accessibility of PM, or its inflammatory biproducts, to otherwise privileged brain regions.

Synergies between air pollution $PM_{2.5}$ and cigarette smoke were shown across the human lifespan for children's body mass index and older adult cardiovascular mortality, lung cancer, and neurodegeneration/cognitive decline (Forman and Finch 2018). For example, the combined effect of cigarette smoke and $PM_{2.5}$ on lung cancer mortality was 2.2 times greater than the expected additive effects of the individual exposures in the U.S. Cancer Prevention Study II (Turner et al. 2014). It was also suggested that diesel emissions and ozone acted synergistically with viruses and airways agonists, respectively (Mauderly and Samet 2009).

The present study leveraged murine experimental models to establish the interactions and joint influence of nanoscale particulate matter (nPM, with aerodynamic diameter ≤200 nm) and CCH secondary to bilateral carotid artery stenosis (BCAS) on white matter neurotoxicity. Investigations demonstrated that nPM exposure generated white matter neuroinflammation (Babadjouni et al. 2018; Woodward et al. 2017a) in cultured cells and murine models, and experimental CCH produced selective white matter structural damage and corresponding behavioral deficits (Liu et al. 2013; Shibata et al. 2004, 2007) in murine models. This study investigated possible synergies of these joint brain insults for white matter injury that exceed the additive effects of the two individual exposures. Experiments then examined the cell types and inflammatory mediators that contribute to this process.

## Methods

### Study Design

The prespecified objective of this study was to investigate potential synergies of nPM and CCH on white matter injury that exceed the additive effects of the two individual exposures. Experiments then sought to examine the specific cell types and inflammatory mediators that contributed to this process. C57BL/6J male mice that were 10 weeks of age were used for this controlled laboratory experiment. Mice were assigned randomly to each of four exposure paradigms [filter (FA), nPM, FA + BCAS, nPM + BCAS; Figure 1]. Animals that died during surgery/perioperatively were excluded from analysis based on prospectively established criteria. Out of 252 mice, 59 mice died perioperatively (23.4%) and were excluded from analysis.

The primary study end point [white matter injury on Klüver-Barrera (KB) staining] and secondary study end points [white matter injury on MRI and histochemistry, glial cell activation, neuroinflammation, oxidative stress, behavioral assessment, and transcriptomic responses (RNA-Seq)] were prospectively selected. Sample size was calculated according to the primary end point (white matter injury; KB). To demonstrate the expected mean group differences for synergism (two-sided alpha = 0.05, 80% power), each arm of the study was determined to require 15 animals according to power analysis. Eighteen animals were included per group to account for uncertainty and variation with respect to sensitivity analysis. Secondary end point analyses were calculated to demonstrate an effect in the joint exposure group that was greater than each of the single-exposure cohorts. No specific intermediate end points were defined to stop data collection. However, per protocol, humane euthanasia was performed immediately if any animal appeared to be in distress at any time during the experiments.

For each end point, the data were collected and processed randomly. All animal caretakers and investigators who performed outcome assessments were blinded to the exposure allocation. No outliers were reported or excluded. Experiments were performed once for each distinct end point. However, multiple markers of white matter injury [KB, dMBP, T2 weighted magnetic resonance imaging (MRI)], inflammation (Iba-1, GFAP, C5, C5α, CD88, TLR4), and oxidative stress (8-OHdG, nitrate, nitrite) were measured in separate experimental cohorts (Table S1). Sample size for each assessed outcome is listed in Table 1. Seven mice in each group (FA, nPM, FA + BCAS, nPM + BCAS) were used for RNA-Seq and quantitative real-time polymerase chain reaction (qPCR) experiments. Sample sizes for each exposure are listed in Table S1.

### Animals

All procedures were performed in accordance with and reviewed by the University of Southern California (USC) Institutional Animal Care and Use Committee (IACUC) and in accordance with the Guide for the Care and Use of Laboratory Animals [National Institutes of Health (NIH)]. Mice were purchased from Jackson Laboratories. No previous procedures had been performed. Animals were housed under USC Department of Animal Resources on a 12-h light:dark cycle (0600 hours to 1800 hours) with free access to food and water (except during the nPM/FA exposure periods). Average husbandry temperature was 22°C (range 20°C to 26°C), with humidity from 30% to 70%. Mice were group housed with four mice per cage, and single mice were randomized to one of four exposure groups listed in the study design section: *a*) FA, *b*) nPM, *c*) FA + BCAS *d*) nPM + BCAS. Mice undergoing behavior testing had specified changes in feeding and housing (see "Behavior" section). After the final exposure, mice were humanely euthanized within 24–72 h by performing a thoracotomy and cardiotomy while animals were under deep anesthesia with an overdose of ketamine [80– 200 mg/kg intraperitoneally (IP)] and xylazine (5–20 mg/kg IP). For immunohistochemistry, mice were then transcardially perfused with phosphate-buffered saline (PBS) with heparin, followed by fixative solution (10% paraformaldehyde in 0.01 mol/L PBS buffer). Brains were stored in paraformaldehyde for 24 h at 4°C, dehydrated in 70% ethanol, and paraffin embedded. For western blot, mice were transcardially perfused with PBS with heparin (without a fixative solution) and brains were fresh frozen with liquid nitrogen and preserved at −80°C. For RNAseq analysis, no perfusion was performed, and brains were frozen with liquid nitrogen and stored at −80°C.
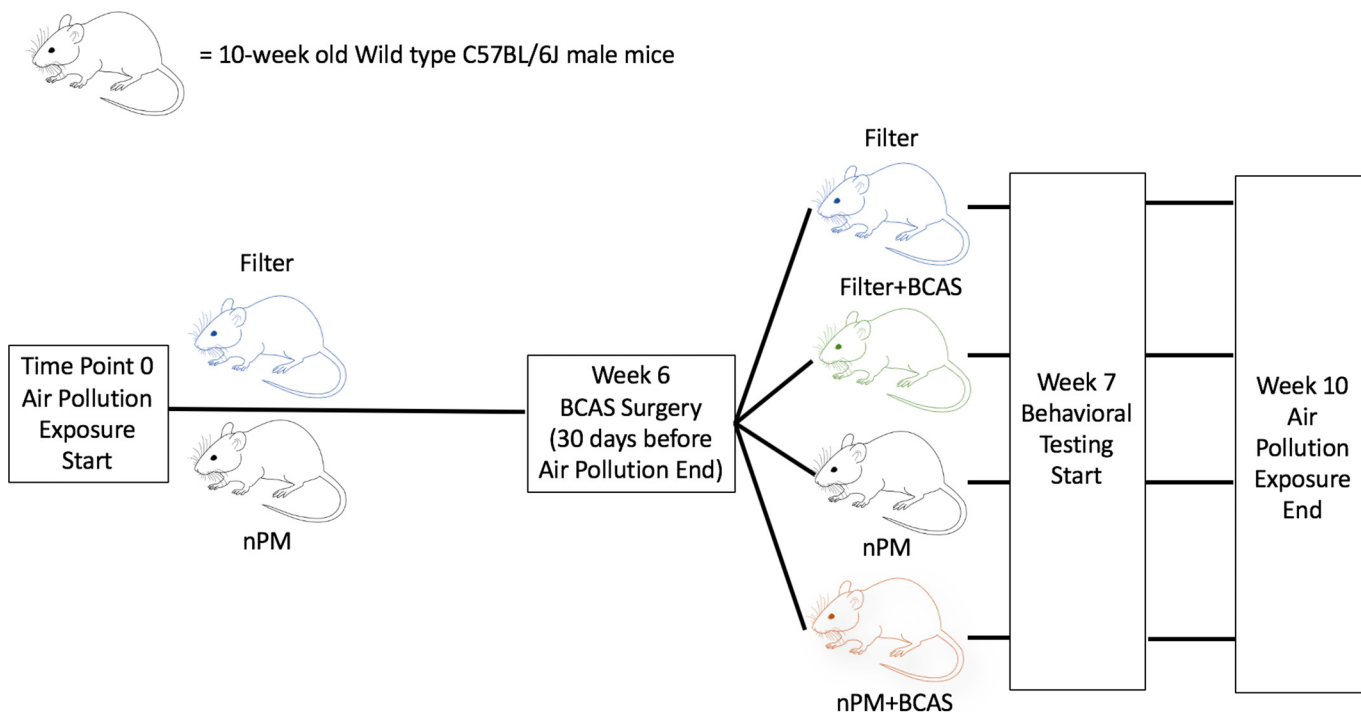
**Figure 1.** Experimental model of BCAS and nPM exposure. Mice begin nPM or FA exposure for 5 h/d, 3 d/wk at time point zero. At week 6 of exposure, BCAS surgery is completed. Eight-arm radial maze testing begins at week 7 followed by NOR testing. The exposure ends at the conclusion of week 10. Note: BCAS, bilateral carotid artery stenosis; FA, filtered air; NOR, novel object recognition; nPM, nanoscale particulate matter.

## PM Collection

nPM was collected in an urban area in central Los Angeles in direct proximity to a busy roadway, primarily impacted by traffic emissions, as previously described (Misra et al. 2002; Woodward et al. 2017a). Briefly, $PM_{0.2}$ was collected at $400 \, \text{L/min}$ flow using a high-volume ultrafine particle sampler that removes particles larger than $0.2 \, \mu\text{m}$ by means of a multiple rectangular (slit) geometry jet conventional impactor. The resulting nPM was collected on pretreated Teflon filters [$8 \times 10$, polytetrafluoroethylene (PTFE), $2 \, \mu\text{m}$ pore] placed directly downstream of the impactor and transferred into an aqueous suspension by soaking in Milli-Q deionized water (total organic compounds $<10 \, \text{ppb}$, particle free, endotoxin $<1 \, \text{unit/mL}$, endotoxin-free glass vials) for 30 min. This process was followed by vortexing for 5 min and sonication for 30 min for resuspension. Endotoxin was not detected in these suspensions (Limulus amebocyte assay: LPS $<0.02 \, \text{EU/mL}$). Fresh sterile filters were extracted in a similar manner to that described above and used as control sample blanks. Aqueous nPM suspensions were pooled and frozen at $-20°\text{C}$ following U.S. Environmental Protection Agency–recommended procedures (Biran et al. 1996).

The size distribution of the aerosol inside the suspension was measured by means of dynamic light scattering (Dynamic Light Scattering BI-200SM; Brookhaven Instruments Inc). To analyze the possibility of agglomeration, two stages of filtration were performed and compared, $1,000 \, \text{nm}$ filtration and $450 \, \text{nm}$ filtration.

## PM Exposure

The nPM suspensions were reaerosolized by means of a HOPE jet nebulizer (Model 11310; B&B Medical Technologies) connected to HEPA-filtered compressed air. This aerosolized stream was mixed with clean air filtered by a HEPA capsule (Model No. 12144, Pall Laboratory), and passed through a diffusion dryer (Model 3620, TSI Inc.) containing prebaked silica gel to remove excess water vapor from the aerosol and decrease the relative humidity (RH) to $\sim 50\%$. The electrical charge of the generated aerosols was also removed by passing through a cylinder supplied with 10 Po-210 neutralizers prior to entering the exposure chambers. Particle size and concentration were continuously monitored throughout the mouse exposure by a scanning mobility particle sizer (SMPS Model 3080, TSI Inc.) in parallel with animal exposure chambers. A total of $15 \, \text{L/min}$ of aerosol flow was generated, with the majority ($10 \, \text{L/min}$) drawn through the exposure chambers and the remaining $5 \, \text{L/min}$ diverted to Teflon and quartz filters for particle collection and characterization. Teflon filters were used for measurement of mass concentration as well as for concentrations of inorganic ions, trace elements, and metals. The mass concentration of nPM was determined by pre- and post-weighing the Teflon filter under controlled temperature and relative humidity. One Teflon filter was extracted with a mixture of ultrapure (Milli-Q®) water and ethanol ($5 \, \text{mL}$: $0.15 \, \text{mL}$, respectively), for analysis of inorganic anions [ammonium ($NH_4^+$), nitrate ($NO_3^-$), and sulfate ($SO_4^{2-}$)] by means of ion chromatography using a Dionex Model DX-500 Ion Chromatograph (Herner et al. 2006). PM-bound metals and trace elements were analyzed by magnetic-sector inductively coupled plasma mass spectroscopy in Thermo Scientific ELEMENT2 High Resolution ICP-MS unit using a microwave-assisted digestion that uses a mixed acid of nitric acid, hydrochloric acid, and hydrofluoric acid (Lough et al. 2005). The complete dissolution of metals present in aerosols is achieved by microwave-assisted acid digestion in Teflon bombs. An automated, temperature- and pressure-regulated, trace analysis microwave system (Milestone Ethos+) is used. The acid chemistry employs a mix of ultra-high-purity acids ($0.6 \, \text{mL} \, 16\text{N} \, HNO_3$, $0.2 \, \text{mL} \, 12\text{N} \, HCl$, $0.1 \, \text{mL} \, 28\text{N} \, HF$). The method is efficient and rapid, with digestion of a 36-sample batch completed in 30 min. Traditionally difficult elements (Cr, noble metals, platinum group) and compounds (aluminosilicates, quartz) are completely solubilized. A typical batch includes 6

**Table 1.** Outcome summary table.

| Outcome | FA | nPM | FA+BCAS | nPM+BCAS | FA vs. nPM | FA vs. FA+BCAS | FA vs. nPM+BCAS | nPM vs. nPM+BCAS | FA+BCAS vs. nPM+BCAS | Synergy p-value | Fold supra-additivity | Sample size |
|---|---|---|---|---|---|---|---|---|---|---|---|---|
| **Behavior** | | | | | | | | | | | | |
| 8-arm radial maze, revisiting errors | 7.4±1.4 | 8.2±0.9 | 6.8±0.5 | 8.8±0.4 | 0.76 | 0.80 | 0.27 | 0.83 | <0.05 | 0.22 | — | 12 |
| 8-arm radial maze, novel entries | 5.4±0.3 | 5.2±0.3 | 5.1±0.1 | 4.8±0.08 | 0.79 | 0.47 | 0.0042 | <0.05 | 0.15 | 0.39 | — | 12 |
| NOR, baseline | 51.1±1.6 | 47.2±1.9 | 49.5±0.78 | 49.6±1.13 | 0.23 | 0.86 | 0.88 | 0.63 | 1.0 | — | — | 12 |
| NOR, short-term | 69.0±4.5 | 57.9±5.3 | 51.8±3.7 | 56.2±3.9 | 0.30 | 0.042 | 0.19 | 0.99 | 0.90 | 0.09 | — | 12 |
| NOR, long-term | 52.1±3.9 | 53.8±3.4 | 52.1±2.3 | 51.1±3.3 | 0.98 | 1.00 | 1.00 | 0.94 | 1.00 | 0.67 | — | 12 |
| **White matter** | | | | | | | | | | | | |
| Klüver-Barrera | 0.31±0.1 | 0.46±0.14 | 0.60±0.12 | 1.33±0.12 | 0.81 | 0.34 | <0.0001 | <0.0001 | 0.0004 | 0.018 | 2.32 | 18 |
| dMBP | 5.2±0.3 | 7.8±0.4 | 7.5±0.23 | 9.6±0.5 | 0.0001 | 0.0005 | <0.0001 | 0.009 | 0.0024 | 0.50 | — | 8[a] |
| **Glial activation** | | | | | | | | | | | | |
| Iba-1 | 96.9±6.8 | 117.9±4.5 | 137.6±8.4 | 161.0±4.7 | 0.05 | 0.0002 | <0.0001 | <0.0001 | 0.093 | 0.85 | — | 18[b] |
| GFAP | 67.8±2.3 | 65.7±2.8 | 107.9±4.5 | 110.9±7.5 | 0.98 | <0.0001 | <0.0001 | <0.0001 | 0.97 | 0.55 | — | 18[b] |
| **Inflammation (whole brain)** | | | | | | | | | | | | |
| TLR4 | 0.6±0.03 | 0.8±0.05 | 1.0±0.08 | 1.3±0.07 | 0.17 | 0.0057 | <0.0001 | 0.0002 | 0.0053 | 0.18 | — | 4 |
| C5 | 0.6±0.04 | 0.9±0.04 | 1.0±0.04 | 1.3±0.09 | 0.0035 | 0.0019 | <0.0001 | 0.0067 | 0.013 | 0.60 | — | 4 |
| C5α | 0.8±0.08 | 1.1±0.07 | 1.4±0.1 | 1.8±0.05 | 0.17 | 0.0028 | <0.0001 | 0.0005 | 0.032 | 0.49 | — | 4 |
| CD88 | 0.7±0.07 | 1.0±0.09 | 1.0±0.02 | 1.3±0.05 | 0.037 | 0.014 | <0.0001 | 0.0086 | 0.022 | 0.84 | — | 4 |
| **Inflammation (corpus callosum)** | | | | | | | | | | | | |
| C5 | 7.5±0.5 | 11.5±0.6 | 9.5±0.8 | 19.8±1.1 | 0.0006 | 0.24 | <0.0001 | <0.0001 | <0.0001 | <0.0001 | 2.05 | 18[c] |
| C5α | 8.2±0.9 | 14.8±1.4 | 12.0±0.8 | 18.5±0.4 | <0.0001 | 0.075 | <0.0001 | 0.072 | 0.0012 | 0.98 | — | 18[c] |
| CD88 | 13.5±1.3 | 16.2±1.1 | 18.5±1.5 | 24.0±2.0 | 0.57 | 0.091 | 0.0002 | 0.0048 | 0.067 | 0.34 | — | 8[a] |
| **Oxidative stress** | | | | | | | | | | | | |
| Nitrate | 10.9±0.7 | 18.8±2.7 | 23.4±4.4 | 91.0±21.2 | 0.94 | 0.83 | <0.0001 | 0.001 | 0.0027 | 0.012 | 3.93 | 4[d] |
| Nitrite | 2.5±0.2 | 3.4±0.3 | 4.0±0.4 | 6.4±0.9 | 0.51 | 0.20 | 0.0005 | 0.0035 | 0.02 | 0.16 | — | 4[d] |
| 8-OHdG | 3.4±0.2 | 5.3±0.2 | 4.8±0.4 | 7.6±0.3 | <0.0001 | 0.0051 | <0.0001 | <0.0001 | <0.0001 | 0.11 | — | 8[a] |
| **MRI** | | | | | | | | | | | | |
| Corpus Callosum Volume | 2.5±0.04 | 2.3±0.08 | 2.1±0.09 | 1.8±0.1 | 0.40 | 0.016 | <0.0001 | 0.0004 | 0.033 | 0.30 | — | 6[e] |

Note: Interaction $p$-values, fold supra-additivities of the nPM + BCAS interaction and post hoc $n$-values for each of the four comparison groups are shown for all outcomes. NOR testing, White matter injury (Klüver-Barrera, dMBP), glial activation (Iba-1, GFAP), inflammation (TLR4, C5, C5α, CD88), oxidative stress (Nitrate, Nitrite, 8-OHdG) and MRI volumes were analyzed using a general linear model with main effects for nPM, BCAS and the nPM + BCAS interaction. Tukey Kramer adjustments were used for pairwise comparisons. For the 8-arm radial maze, a repeated measures analysis with mixed effect models was used to analyze effects of groups and blocked trial number. Mean slope was analyzed using a linear mixed effects model with main effects for nPM, BCAS and the nPM + BCAS interaction (synergy). Data represented as mean ± standard error. Sample size represents number in each of the four groups. Mice were used for multiple end points; see Table S1. Data displayed in Figures 2–5 and 7. Iba-1, GFAP cell count were assessed using immunohistochemistry. dMBP, 8-OHdG, and inflammation in the corpus callosum (C5, C5α, CD88) were assessed using immunofluorescent staining. Inflammatory markers in the whole brain (TLR4, C5, C5α, CD88) were assessed with western blots. Nitrite and nitrate concentrations were assessed with a colorimetric assay using the Griess Reaction. Table S7 lists outcomes for mice that underwent behavioral testing. Units: NOR (discrimination index %); Klüver-Barrera (white matter injury score); Iba-1, GFAP (positive cells/0.1 mm²); dMBP, 8-OHdG, inflammation in the corpus callosum (C5, C5α, CD88) (integrated density/μm²); inflammation in the whole brain (TLR4, C5, C5α, CD88) (density (relative to GAPDH)); nitrite, nitrate (μM). —, no data available; BCAS, bilateral carotid artery stenosis; C5, complement component 5; C5α, complement component 5α; CD88, complement component C5α receptor 8, dMBP, degraded myelin basic protein; FA, filtered air; GFAP, glial fibrillary acidic protein; Iba-1, ionized calcium-binding adaptor protein-1; NOR, novel object recognition; nPM, nanoscale particulate matter; TLR4, Toll-like receptor 4; 8-OHdG, 8-oxo-2′-deoxyguanosine.

[a]$n = 7$ in nPM + BCAS.

[b]$n = 12$ in FA + BCAS nPM + BCAS.

[c]$n = 12$ in FA + BCAS, $n = 13$ in nPM + BCAS.

[d]$n = 5$ in nPM.

[e]$n = 5$ in FA + BCAS.

standard reference materials (SRMs), 4 matrix blanks, 2 method blanks, and 2 matrix spikes. The SRMs used to monitor digestion performance were selected to represent phases that represent actual aerosols or significant aerosol components. These included the NIST SRMs: Recycled Auto Catalyst (#2556), Urban Dust (#1649a), and San Joaquin Soil (#2709).

Water-soluble organic carbon (WSOC) was measured by extracting the quartz filters in high-purity water followed by analysis by means of a Shimadzu TOC-V CSH/CSN. Total Organic Carbon Analyzer WSOC is quantified in this method by a nondispersive infrared detector (NDIR) after catalytic conversion of OC to $CO_2$ at 680°C. Inorganic carbon in the water extracts is eliminated prior to analysis by acidification (HCl) and sparging (zeroair). Calibration curves (potassium hydrogen phthalate) followed by two MQ blanks were run every 10 samples. Quantification limits are in the range of $40–80\,\mu g\,L^{-1}$ $(40–80\,ng\,m^{-3})$. Analytical precision for this method typically falls in the range of 1%–4% RSD (Zhang et al. 2008).

Mice were exposed to either reaerosolized nPM or FA for 5 h per day, 3 d per week for 10 wk (150 total hours) (Figure 1). Exposures were conducted in temperature- and air-controlled sealed whole-body chambers with adequate ventilation. Multiple cohorts of mice were used in a series of comparable exposures.

### BCAS

BCAS procedures (Liu et al. 2013; Shibata et al. 2004) were performed 30 d prior to the conclusion of nPM/FA exposure (Figure 1). Rectal temperature was maintained at 36.5°C–37°C. Mice were anesthetized by IP ketamine/xylazine and placed in the prone position. Cerebral blood flow (CBF) values were monitored with a microtip fiber probe (Probe 418-1 master probe PF 5010 Laser Doppler Perfusion Monitoring Unit, Perimed AB) fixed to the skull 1 mm posterior and 5 mm left of bregma. The mouse was then rotated to the supine position, and bilateral common carotid arteries were exposed through a midline cervical incision. A 0.18 mm diameter microcoil (Sawane Spring Co., Ltd.) was applied to one carotid artery. CBF was recorded after the first coil application. A second microcoil was applied to the other carotid artery, and CBF was recorded again. The incision was closed, and the mouse recovered in a temperature-controlled environment. Carprofen (5 mg/kg) was given subcutaneously at 24 and 48 h postoperatively.

### Behavior

***8-Arm radial maze testing.*** Twelve mice in each exposure group (FA, nPM, FA + BCAS, nPM + BCAS) were designated for behavioral testing. The order of animal testing was randomized for each behavior test. The 8-arm radial maze, a test of spatial working memory, was initiated 21 d prior to the conclusion of nPM/FA exposure (Figure 1) and modified from previously described testing (Shibata et al. 2007). Each mouse was individually housed and underwent food deprivation for 7 d prior to the initiation of behavioral testing with an allowance of 2.5 g of food per day to reduce initial body weight by 10%–15%. Restricted feeding was continued during behavioral testing. On pretrial day 1, the mouse was allowed 5 min of free exploration with each arm of the 8-arm radial maze baited with Fruity Pebbles™ food pellets. On pretrial day 2, the mouse was placed in the center of the maze and trained to interact with the door apparatus. On trial days 1–16, each arm of the maze was baited with food pellets, and the mouse was placed in the center of the maze. The mouse was allowed to make an initial arm choice, defined by advancing at least 5 cm into the arm. The other 7 arms were then closed. On exiting the chosen arm, the mouse was confined to the center for

5 s by closing the remaining arm door. After the 5-s delay, all doors were opened, and the mouse was allowed to make a new choice. When the mouse had retrieved all 8 pellets, or 25 min had elapsed, the trial was ended. One trial per mouse was conducted every day for 16 d. A single session or blocked trial consisted of two trials performed on consecutive days. Time between trials was 24 h in a given blocked trial for each mouse.

At the end of each trial, the radial maze was cleaned with 70% ethanol to minimize olfactory cues. For each trial, revisiting errors and arm choices within the first eight entries were recorded. Performance was evaluated daily by an observer blinded to treatment group. Data is expressed as mean values over 2 blocked trials (performed on consecutive days), for a total of 8 blocked trials.

### *Novel Object Recognition Testing*

Novel object recognition (NOR) testing was performed on the final 3 d of the nPM/FA exposure (Figure 1). The same cohort of mice that underwent testing in the 8-arm radial maze was used for NOR (following 8-arm radial maze testing). On the day prior to testing, mice were individually habituated in a dimly lit black Plexiglas® box (38 cm × 38 cm × 38 cm) for 15 min. On testing day 1, mice were allowed to explore sample/familiar objects—two yellow plastic cylinders (8 cm × 2 cm), A-A, symmetrically placed 6 cm from the nearest walls—for 15 min. Short-term memory was assessed 90 min later by changing configuration A-A to configuration A-B, with B being a purple figure (8 cm × 3 cm × 3 cm). Mice were placed in the same position as the prior trial to minimize potential confounds with spatial memory, and behavior was recorded for 5 min. Long-term memory was assessed 24 h later by changing the configuration to A-C, with C being a red triangular wooden block (4 cm × 4 cm × 8 cm). Again, behavior was recorded for 5 min. The objects and testing apparatus were thoroughly cleaned with 70% ethanol at the end of each trial. All trials were videorecorded by a camera (Logitech HD Pro Webcam920 with Smart3.0 Software; Panlab Harvard Apparatus) positioned above the testing apparatus. In each trial, time spent exploring the familiar (F) object (A) and the new (N) object (B/C) was recorded and assessed by a grader blinded to exposure conditions. Exploration behavior was defined as sniffing or touching the object at a distance of <2 cm from the snout. Discrimination index quantifies the amount of time the mouse spends exploring the novel object in comparison with the total time exploring the novel or familiar object. A lower index indicates a deficit in this test. Discrimination index was calculated as N/(N+F) for intergroup comparison (Bevins and Besheer 2006; Ennaceur and Delacour 1988).

### *MRI*

MRI scans used a 7T PET-MR system (MR Solutions Ltd.) with a standard 20-mm internal diameter quadrature birdcage mouse head coil with a setup described in our earlier publications (Montagne et al. 2018). For *in vivo* scans the animals were anesthetized with 1.5%–2.0% Isoflurane/air and monitored for respiration with an abdominal pressure-sensitive probe (80–100 BPM) and temperature with a rectal probe (36.5°C ± 0.5°C) to ensure reproducible deepness of anesthesia (Équipement Vétérinaire MINERVE mouse imaging cell). T2-weighted anatomical images were collected using 2D-fast spin echo sequence (FSE, TR/TE 4,600/28 ms, 40 slices, slice thickness 500 μm, in-plane resolution $100 \times 50\,\mu m^2$). The volumetric analysis was performed using ImageJ by an observer blinded to treatment group. Corpus callosum was manually outlined using four consecutive sections from the anterior brain corresponding to the area used

for immunohistochemistry. The outlined area was measured and multiplied by slice thickness and number of slices. All analyses were performed by investigators blinded to both the nPM and BCAS type of exposure. The data are presented as cubic millimeters.

### Protein Analysis by Western Blot

After brains were harvested, protein was extracted. Brains were weighed ($\sim 300$ mg) and suspended in 1 mL NPER Reagent buffer (Product #87792, Thermo Scientific) containing protease inhibitors (Roche complete mini protease inhibitor cocktail tablets #04693124001, Sigma). Tissue was then disrupted using a homogenizer on setting 6 (Tissue Tearor #985370, Cole Parmer) and incubated on ice for 10 min. Lysates were cleared by centrifugation at $10,000 \times g$ for 10 min. Protein concentration of the resulting supernatant was measured using Pierce BCA Protein Assay Kit. Brain tissue lysates with total protein of 50 μg were separated by SDS-PAGE, transferred to a nitrocellulose membrane, and blocked in 5% nonfat milk for 1 h. Blots were incubated overnight in primary antibody C5, C5α, CD88, and TLR4 (Table S2). After washing with TBS-Tween™-20, blots were incubated in appropriate secondary antibodies (Table S2) in 5% nonfat milk in TBS-Tween™-20. Blots were developed with GE Health Care ECL prime western blotting detection reagent and imaged using a CCD camera (G:BOX, Syngene; image resolution 4 megapixels). Density of proteins of interest were normalized to GAPDH (Table S2). The observer was blinded to treatment group.

### KB Histochemistry for White Matter Injury

A section of the brain located from 1 mm anterior to the bregma to 2 mm posterior to the bregma (adjusted according to mouse atlas) was sliced into serial 3-μm-thick coronal sections. KB staining was performed on the slice located at the bregma. Paraffin-embedded slides were deparaffined and hydrated from 100% to 95% alcohol. Sections were immersed in Luxol® fast blue solution and incubated in an oven at 56°C overnight. Excess stain was then removed by a rinse with 95% alcohol, followed by distilled water. Sections were differentiated singly in lithium carbonate solution for 30 s. Differentiation was continued in 70% alcohol until gray matter was clear and white matter sharply defined. Slides were then placed in distilled water, counterstained with cresyl violet acetate, and dehydrated. Slides were mounted with resinous medium and visualized using BZ-9000 brightfield microscopy (Keyence) at 400×. White matter changes in the medial corpus callosum were graded as follows: grade 0 is normal, grade 1 demonstrates disarrangement of nerve fibers, grade 2 has the formation of marked vacuoles, and grade 3 involves disappearance of myelinated fibers (Wakita et al. 1994). The left medial corpus callosum and right medial corpus callosum were assigned numeric scores, and the two values then averaged. Average scores from two independent, blinded observers were calculated for each mouse. The two observers' scores were then averaged for a final score.

### Immunohistochemistry and Immunofluorescence

Immunohistochemistry and immunofluorescence were performed on coronal slices of 5-μm thickness from the same coordinates as above. Paraffin-embedded sections were deparaffined and rehydrated with graded alcohol solutions ranging from 100% to 70%. Sections were stained for ionized calcium binding adaptor molecule 1 (Iba-1), glial fibrillary acidic protein (GFAP), degraded myelin basic protein (dMBP), complement C5, C5α, CD88, and 8-hydroxydeoxyguanosine (8-OHdG) (Table S3). After antigen retrieval, sections were blocked in 5% goat (Iba-1, GFAP) for immunohistochemistry or donkey (dMBP, C5, C5α, CD88, 8-OHdG) serum for immunofluorescence. Sections were incubated overnight with primary antibody, followed by incubation with appropriate secondary antibody (Table S3).

Iba-1 and GFAP were visualized using a BZ-9000 microscope (Keyence). The number of GFAP or Iba-1 positive cells, above a specified size filter, were counted in one high-powered field (400×) of the left and right medial corpus callosum for each animal, and the two values were averaged.

Immunofluorescent sections were co-stained with Hoechst 33342 (for nuclei, 1:5,000; Life Technologies). Slides were mounted with Dako fluorescent mounting media, cover-slipped, and visualized using BZ-9000 fluorescent microscopy (Keyence). Mean fluorescent density was quantified in one high-powered field (200×) of the left and right medial corpus callosum for each animal, and the two values were averaged. Average scores from two independent, blinded observers were calculated for each mouse. Image analysis was performed using NIH Image J software. Protocols followed NIH Image J user guide.

### Nitrite and Nitrate Assay

Nitrite and nitrate of whole brain tissue lysates were colorimetrically assayed [OxiSelect™ In Vitro Nitric Oxide (Nitrite/Nitrate) Assay Kit (Cell BioLabs)]. Brain was homogenized by tissuetearor (model 985370) in N-Per extraction buffer in ice and centrifuged $14,000 \times g$ for 15 min in 4°C to obtain supernatants for assay. Nitrite concentration was determined by the Griess reaction, which converts nitrite to a colored azo dye product with absorbance at 540 nm, per the manufacturer's instructions (STA-802, Cell BioLabs). Briefly, tissue samples, PBS, and Griess Reagent A (Part No. 280205, Cell BioLabs) were added to each well of a 96-well microtiter plate. Griess Reagent B (Part No. 280,206, Cell BioLabs) was then added to each well, and the plate was incubated at room temperature for 10 min. Nitrate concentration was determined by nitrate reduction to nitrite followed by the Griess reaction. To measure nitrate concentration, tissue samples and the Enzyme Reaction Mixture (Enzyme Mixture: Part No. 280204; Enzyme Cofactor: Part No. 280205; Cell BioLabs) were added to each well of a 96-well microtiter plate. The plate was incubated at room temperature for 1 h. Griess Reagent A (Part No. 280205; Cell BioLabs) and Griess Reagent B (Part No. 280206, Cell BioLabs) were then added to each well and the plate was incubated at room temperature for 10 min. Absorbance was imaged using a Bio-Rad model 680 microplate reader. Nitrite and nitrate concentrations were analyzed by comparing the sample absorbance at 540 nm to the standard curve. The observer was blinded to treatment group.

### RNA-Seq and Data Analysis

Following euthanasia, mouse corpus callosum tissue was microdissected under the operating microscope and frozen fresh. To assess gene expression profiles, RNA-Seq was performed on high-quality RNA extracted from fresh frozen samples of individual biological replicates using RNeasy Plus Universal purification kit (QIAGEN); RNA quality control used the Agilent 2100 bioanalyzer (Agilent Technologies). Individuals performing RNA-Seq analysis were blinded to treatment group.

Libraries for RNA-Seq were prepared with the KAPA Stranded RNA-Seq Kit (Kapa Biosystems). The workflow proceeded with mRNA enrichment, cDNA generation and end repair to generate blunt ends; A-tailing; adaptor ligation; and library amplification via high fidelity, low-bias PCR. Different adaptors (Kapa Biosystems) were used for multiplexing samples in one

lane. Libraries were sequenced using an Illumina HiSeq 3000 (SR 1 ×50 bp) (Illumina). Data quality measurements were obtained from the Illumina Sequencing Analysis Viewer (version 2.1.8). Demultiplexing was performed with Illumina Bcl2fastq2 conversion software (version 2.17) program to generate FASTQ file formats for downstream analysis.

Read mapping was then performed within the Illumina BaseSpace™ work environment (RNA-Seq Alignment application), using TopHat 2 (Bowtie 2), aligning reads to the reference genome Mus musculus (UCSC version mm10). Differentially expressed genes were then identified using DESeq2 (version 1.6.3). Network analyses were performed and pathways generated through the use of Ingenuity Pathway Analysis (QIAGEN Inc., https://www.qiagenbioinformatics.com/products/ingenuitypathway-analysis; Krämer et al. 2014) imputing data with a more inclusive *q* value of 0.10 or less.

## qPCR

qPCR was performed on the same corpus callosum tissue sample used for RNA-Seq (separate piece). cDNA was synthesized from total RNA using reverse transcription reagent from BioPioneer Inc., and qPCR was conducted using qPCR master mix (BioPioneer Inc.) in a Bio-Rad Real Time PCR system. The primer pairs used for GAPDH and other genes are listed in Table S4. The following reaction conditions were used: 95°C, 5min; denature at 94°C for 15 s, anneal at 64°C for 10 s, extension at 72°C for 25 s, for 42 cycles. Fluorescent signal was captured at the extension stage.

The qPCR data was analyzed by using comparative or $\Delta\Delta C_T$ method. In brief, Ct values of target genes were normalized to that of GAPDH ($\Delta C_T$), and the $\Delta C_T$ difference between control and treatment was calculated ($\Delta\Delta C_T$), then $\Delta\Delta C_T$ values were transformed to the linear induction fold ($2^{\Delta\Delta CT}$). Log2 fold change was calculated from the linear induction fold.

## Statistical Analyses

PM concentrations were evaluated midway through each exposure period and reported as arithmetic means across the exposure campaign days with less than 10% variation. PM concentrations for each exposure batch were averaged and plotted as a distribution of all exposures. Particle number (PN) concentrations were measured at the beginning of each exposure period. The particle number mean values were calculated as geometric means of the five exposures. Histochemistry, western blot, MRI, and NOR were analyzed using a general linear model with main effects for nPM, BCAS, and the nPM + BCAS interaction (testing for synergy). Pairwise comparisons used Tukey Kramer adjustment for multiple comparisons. Two-tailed unpaired Student's *t*-tests were used to evaluate the effect of behavioral testing/food deprivation on histological analysis. For the 8-arm radial maze, a repeated measures analysis with mixed effect models (over 8 averaged blocked trials) was used to analyze effects of groups and blocked trial number. These models were run in two ways: *a*) a one-factor model compared the four groups (FA, nPM, FA + BCAS, nPM + BCAS) over the eight trials; and *b*) a two-factor model analyzed the main effects for nPM, BCAS, and the nPM + BCAS interaction over the eight trials. Mean slope (linear trend in the behavior outcome over trials) was analyzed using a linear mixed effects model with main effects for nPM, BCAS, and the nPM + BCAS interaction (synergy). For the NOR test, a one-way analysis of variance (ANOVA) was used to analyze baseline behavior between cohorts. Statistics were performed using SAS (Version 9.4, SAS Institute Inc.) and GraphPad Prism (Version 9.1.0, GraphPad Software). Data are presented as mean ± standard error (SE). Alpha level of 0.05 was chosen for statistical significance. For RNA-Seq, results were prioritized according to false discovery rate adjusted *p*-value (*q*-value), with a level of 0.05 for significance.

## Results

### nPM Exposure and Composition

Table S1 demonstrates which nPM exposure batch was used for each experiment. When multiple exposures were used for a specific end point, similar numbers of mice from each exposure batch were included in each treatment group. Overall, the average mass concentration in the inhalation exposure system during the 150 h of the exposure was $305.6 \pm 11.7\,\mu g/m^3$, whereas the average particle number concentration (PNC) of the reaerosolized nPM was $361,703 \pm 8,191\,particles/cm^3$. Total organic matter (TOM) was the most predominant chemical species, accounting for $40.1 \pm 13.9\%$ of the total mass. The mass fractions of trace elements and metals (units of nanograms per microgram of PM mass) are listed in Table S5 for each nPM exposure batch. The average particle size distribution of the exposure aerosol is presented in Figure S1. The size distribution of the aerosol inside the suspension was very similar to the exposure aerosol (see Figure S2). The number concentration was dominated by ultrafine size ranges. Only about 5% of the total number concentration was in the ranges above 243 nm. The aerosol mode diameter was also below 100 nm

### Weight, CBF, and Mortality

Mice in each of the four exposure groups (FA, nPM, FA + BCAS, nPM + BCAS) did not differ in weight throughout the study [means (± SEM) in grams: FA 109.3 (± 1.1) vs. nPM 109.1 (± 0.58) vs. FA + BCAS 108.2 (± 0.87) vs. nPM + BCAS 106.7 (± 0.86), *p* = 0.24], except as planned and described in the behavioral assays. Mean cerebral blood flow (CBF) change did not differ between FA + BCAS (35%) and nPM + BCAS (33%) (*p* = 0.65). Total mortality in all groups was 23.4% (59 mice out of 252). Mortality occurred only in the BCAS groups. Mortality only in the BCAS groups was 41.3% (59 mice out of 143). Surgical mortality after BCAS surgery did not differ between groups (FA + BCAS 41%, nPM + BCAS 41%, *p* = 0.51, see Table S1).

### Behavioral Effects on End Points

In exposures 1 and 2, 12 mice in each of the FA and nPM groups underwent behavioral testing, whereas a simultaneous group of 6 mice in each of the FA and nPM groups did not. There were no significant differences in assessed outcomes between mice that underwent behavioral testing and mice that did not [KB (*p* = 0.70), Iba-1 (*p* = 0.25), GFAP (*p* = 0.73), C5 (*p* = 0.73), and C5α (*p* = 0.34)] (Table S6). Differences between groups remained the same when mice that underwent behavioral testing were compared with all analyzed mice (Table 1; Table S7).

### White Matter Damage in the Corpus Callosum

Mice in the joint nPM + BCAS group had a mean white matter injury score 329% higher than those in the FA group (1.33 ± 0.12 vs. 0.31 ± 0.1). This difference between the mean nPM + BCAS and FA (1.33 − 0.31 = 1.02) scores was 2.32 times higher than the sum of the differences (0.15 + 0.29 = 0.44) between the mean nPM and FA (nPM-FA: 0.46 − 0.31 = 0.15) and FA + BCAS and FA (FA + BCAS-FA: 0.60 − 0.31 = 0.29) (Table 1; Figure 2A,C).
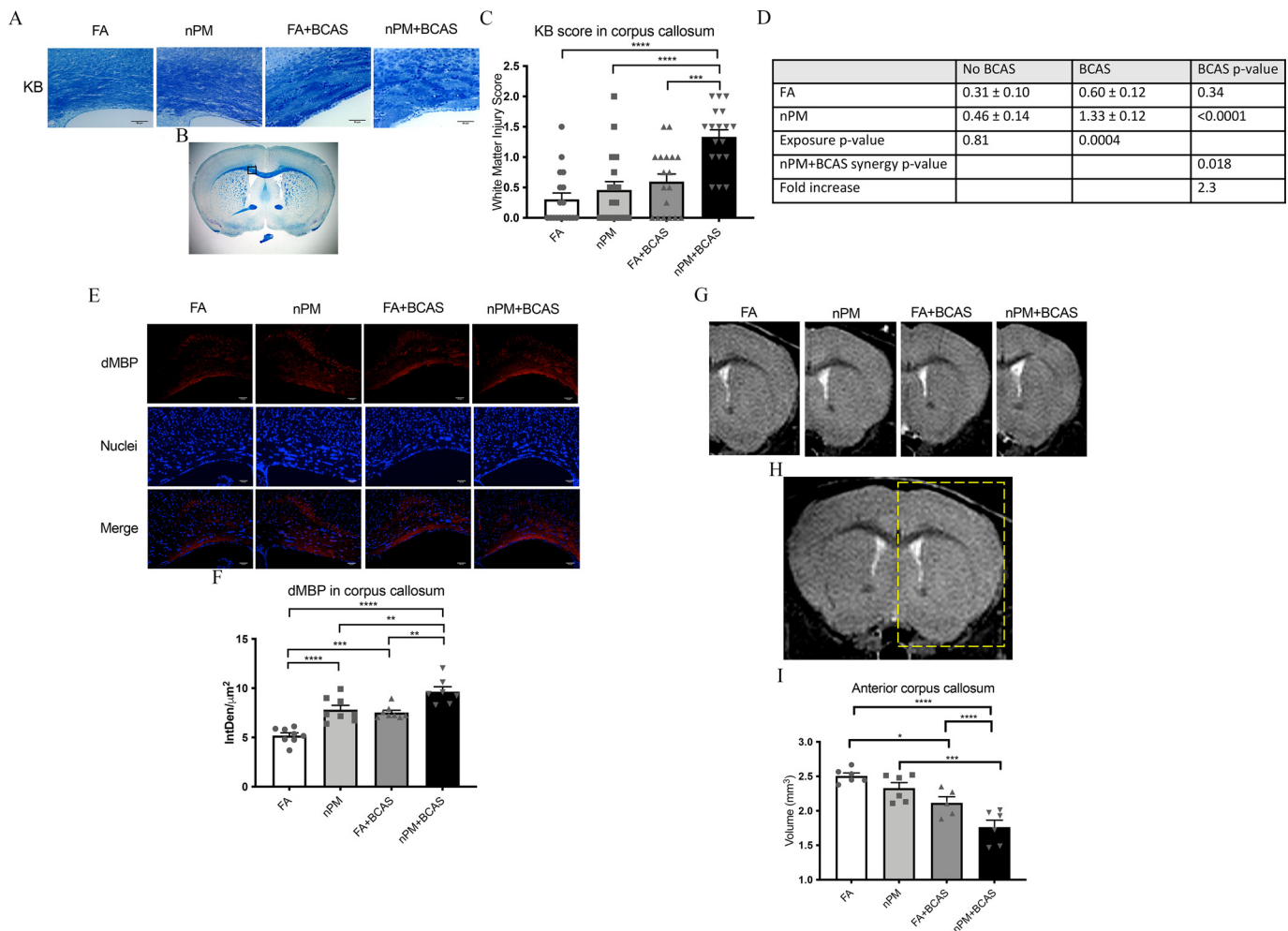
**Figure 2.** Measures of white matter damage in the corpus callosum of mice exposed to nPM or FA with or without BCAS. (A) Representative corpus callosum Klüver-Barrera staining of mice in each experimental group (400×). (B) Representative image of region analyzed at low magnification (Scoring on right/left. Right demarcated.). (C–D) White matter injury score in mice exposed to nPM or FA with or without bilateral carotid artery stenosis (BCAS) ($n = 18$/group; numbers are mean ± standard error). General linear model with main effects for nPM, BCAS, nPM + BCAS interaction was used to calculate the synergy p-value in D. Exposure and BCAS p-values were calculated using the Tukey Kramer adjustment. (E) Representative images of degraded myelin basic protein (dMBP; red) immunofluorescence and nuclei (blue) in the corpus collosum of mice in each experimental group (200×). Analysis performed on both right/left side (right region demarcated in B). (F) dMBP immunofluorescent density in the corpus collosum of mice in each experimental group. (G) Representative T2 weighted images of the corpus callosum of mice in each experimental group. (H) T2 weighted representative MR image of region of interest in the corpus callosum. Yellow dashed square indicates insert in G. (I) Corpus callosum volume in mice exposed to nPM or FA with or without BCAS. Data represented as mean ± standard error. Scale bars in images represent 50 μm. (A–D) $n = 18$ FA, 18 nPM, 18 FA + BCAS, 18 nPM + BCAS. (E–F) $n = 8$ FA, 8 nPM, 8 nPM, 8 FA + BCAS, 7 nPM + BCAS. (G–I) $n = 6$ FA, 6 nPM, 5 FA + BCAS, 6 nPM + BCAS. General linear model with main effects for nPM, BCAS, nPM + BCAS interaction were used; pairwise comparisons used Tukey Kramer adjustment. Summary data is provided in Table 1. Note: BCAS, bilateral carotid artery stenosis; dMBP, degraded myelin basic protein; FA, filtered air; KB, Klüver-Barrera; nPM, nanoscale particulate matter. $^*p < 0.05$, $^{**}p \leq 0.01$, $^{***}p \leq 0.001$, $^{****}p \leq 0.0001$.

Mice exposed to nPM + BCAS had significantly higher dMBP density in comparison with FA-, nPM-, or FA + BCAS-exposed mice. The joint nPM + BCAS group demonstrated an 85% higher dMBP density in comparison with the FA cohort ($9.6 \pm 0.5$ vs. $5.2 \pm 0.3$) but did not demonstrate a synergistic interaction with respect to dMBP density (Table 1; Figure 2E,F).

### Corpus Callosum Volumes on MRI

BCAS and nPM exposure resulted in smaller corpus callosum volumes on MRI. On T2 weighted MRI, there was no significant difference in corpus callosum volumes between the FA and nPM groups. However, nPM + BCAS-exposed mice had significantly smaller volumes than the FA + BCAS-exposed mice. Volumes were smaller in nPM + BCAS-exposed mice when compared with the FA, nPM, and FA + BCAS groups. The joint nPM + BCAS group had a 30% lower corpus callosum volume when compared with the FA cohort ($1.8 \pm 0.1$ vs. $2.5 \pm 0.04$) but did

not demonstrate a synergistic interaction with respect to corpus callosum volumes (Table 1; Figure 2G,I).

### Glial Cell Activation in the Corpus Callosum

Mice exposed to nPM + BCAS had significantly higher reactive central nervous system (CNS) myeloid (Iba-1 positive) cell counts, such as microglia compared with the FA- and nPM-exposed groups. Additionally, mice in each of the nPM and FA + BCAS groups had significantly higher reactive Iba-1 positive cell counts when compared with the FA-exposed group. The joint nPM + BCAS group mice had 66% higher Iba-1 positive cell counts when compared to the FA cohort ($161.0 \pm 4.7$ vs. $96.9 \pm 6.8$) but did not demonstrate a synergistic interaction with respect to reactive Iba-1 cell counts (Table 1; Figure 3A,B).

Mice exposed to FA + BCAS had significantly higher reactive astrocyte (GFAP positive) cell counts in the corpus callosum in
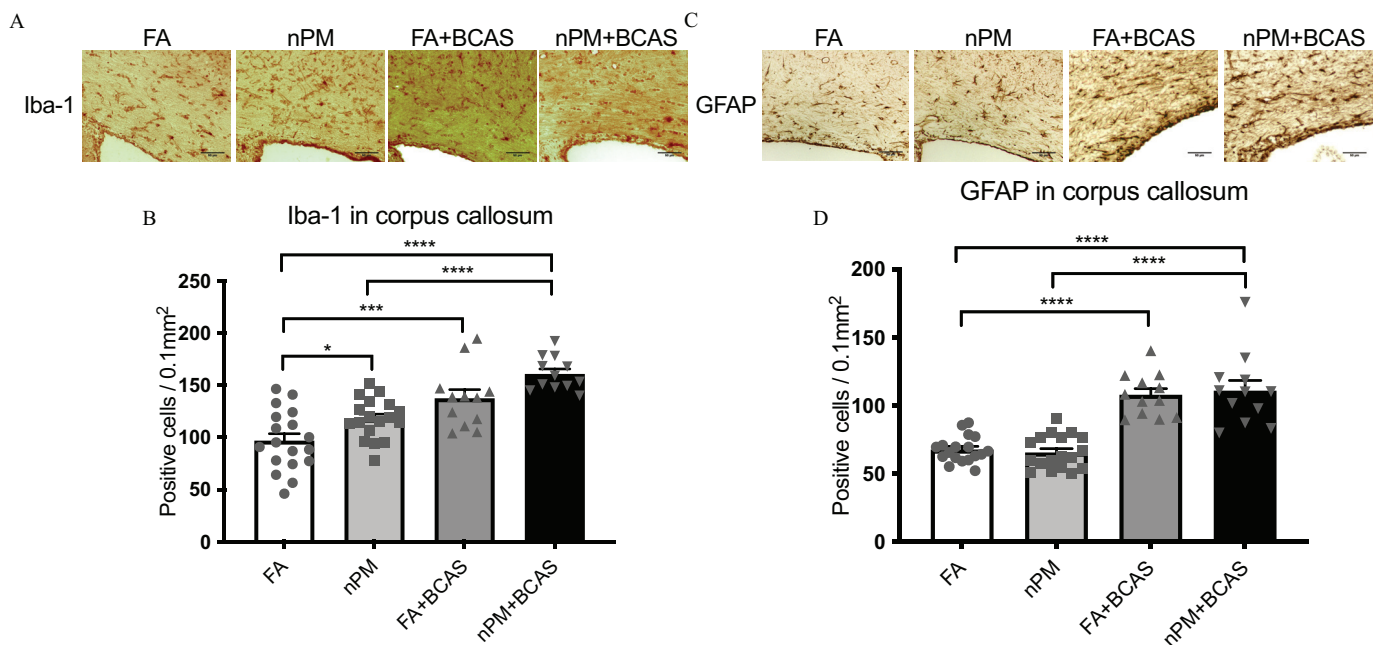
**Figure 3.** Measures of immune cell activation in the corpus callosum of mice exposed to nPM or FA with or without BCAS. (A) Representative images of Iba-1 immunohistochemistry in the corpus callosum of mice in each experimental group (400×). (B) Iba-1 positive cell counts in the corpus callosum of mice in each experimental group. (C) Representative images of GFAP immunohistochemistry in the corpus callosum of mice in each experimental group (400×). Analysis was performed on both right/left side (location of right region is demarcated area in Figure 2B). (D) GFAP positive cell counts in the corpus callosum of mice in each experimental group. Data in graphs represented as mean ± standard error. Scale bars represent 50 μm. Error bars represent standard error. *n* for all panels = 18 FA, 18 nPM, 12 FA + BCAS, and 12 nPM + BCAS. General linear model with main effects for nPM, BCAS, and the nPM + BCAS interaction (testing for synergy) were used. Pairwise comparisons used Tukey Kramer adjustment for multiple comparisons. Summary data is provided in Table 1. Note: BCAS, bilateral carotid artery stenosis; FA, filtered air; GFAP, glial fibrillary acidic protein; Iba-1, ionized calcium-binding adaptor protein-1; nPM, nanoscale particulate matter. $^*p < 0.05$, $^{**}p \leq 0.01$, $^{***}p \leq 0.001$, $^{****}p \leq 0.0001$.

comparison with FA mice. Further, mice exposed to nPM + BCAS had significantly higher reactive astrocyte cell counts in comparison with nPM-exposed mice. However, mice exposed to nPM did not have higher reactive astrocyte cell counts when compared with FA-exposed mice. The joint nPM + BCAS group mice had 64% higher GFAP positive astrocyte cell when compared with the FA cohort ($110.9 \pm 7.5$ vs. $67.8 \pm 2.3$) but did not demonstrate a synergistic interaction with respect to GFAP positive cell counts (Table 1; Figure 3C,D).

### Inflammation in the Brain and Corpus Callosum

Mice exposed to nPM + BCAS had significantly higher TLR4, C5, C5α, and CD88 densities on whole brain western blot analysis in comparison with FA-, nPM-, or FA + BCAS-exposed mice. The joint nPM + BCAS group demonstrated 117% higher TLR4 density ($1.3 \pm 0.07$ vs. $0.6 \pm 0.03$), 117% higher C5 density ($1.3 \pm 0.09$ vs. $0.6 \pm 0.04$), 125% higher C5α density ($1.4 \pm 0.1$ vs. $0.8 \pm 0.08$), and 86% higher CD88 density ($1.3 \pm 0.05$ vs. $0.7 \pm 0.07$) when compared with the FA cohort but did not demonstrate synergistic interactions with respect to these markers in the whole brain analysis (Table 1; Figure 4A–E).

The joint nPM + BCAS group demonstrated 164% higher C5 density in the corpus callosum when compared with the FA cohort [$19.8 \pm 1.1$ vs. $7.5 \pm 0.5$; (Table 1; Figure 4F,G)]. The difference between the mean nPM + BCAS and FA densities ($19.8 - 7.5 = 12.3$) was 2.05 times higher than the sum of the differences ($4.0 + 2.0 = 6.0$) between the mean nPM and FA (nPM-FA: $11.5 - 7.5 = 4.0$) and FA + BCAS and FA densities (FA + BCAS-FA: $9.5 - 7.5 = 2.0$) (Table 1; Figure 4F,G).

Further, mice exposed to nPM + BCAS had significantly higher C5α densities in the corpus callosum when compared with FA- or FA + BCAS-exposed groups. The joint nPM + BCAS

group demonstrated 126% higher C5α density when compared with the FA cohort ($18.5 \pm 0.4$ vs. $8.2 \pm 0.9$) but did not demonstrate a synergistic interaction with respect to C5α density (Table 1; Figure 4H,I).

Mice exposed to nPM + BCAS had significantly higher CD88 density in the corpus callosum in comparison with FA- and nPM-exposed mice. The nPM + BCAS mice demonstrated a trend toward higher CD88 density when compared with FA + BCAS-exposed mice. The joint nPM + BCAS group demonstrated 78% higher CD88 density when compared with the FA cohort ($24.0 \pm 2.0$ vs. $13.5 \pm 1.3$) but did not demonstrate a synergistic interaction with respect to CD88 density (Table 1; Figure 4J,K).

### Oxidative Stress in the Brain and Corpus Callosum

The joint nPM + BCAS group mice had 735% higher whole brain nitrate concentration when compared with the FA cohort [$91.0 \pm 21.2$ vs. $10.9 \pm 0.7$; Table 1; Figure 5B]. The difference between the mean nPM + BCAS and FA nitrate concentrations ($91.0 - 10.9 = 80.1$) was 3.93 times higher than the sum of the differences ($7.9 + 12.5 = 20.4$) between the mean nPM and FA (nPM-FA: $18.8 - 10.9 = 7.9$) and FA + BCAS and FA nitrate concentrations (FA + BCAS-FA: $23.4 - 10.9 = 12.5$) (Table 1; Figure 5B).

Mice exposed to nPM + BCAS had higher whole brain nitrite concentrations in comparison with FA-, nPM-, or FA + BCAS-exposed groups. The joint nPM + BCAS group mice had 156% higher nitrite concentrations when compared with the FA cohort ($6.4 \pm 0.9$ vs. $2.5 \pm 0.2$) but did not demonstrate a synergistic interaction with respect to nitrite concentrations (Table 1; Figure 5A).

Mice exposed to nPM + BCAS had significantly higher corpus callosum 8-OHdG density in comparison with FA-, nPM-, or
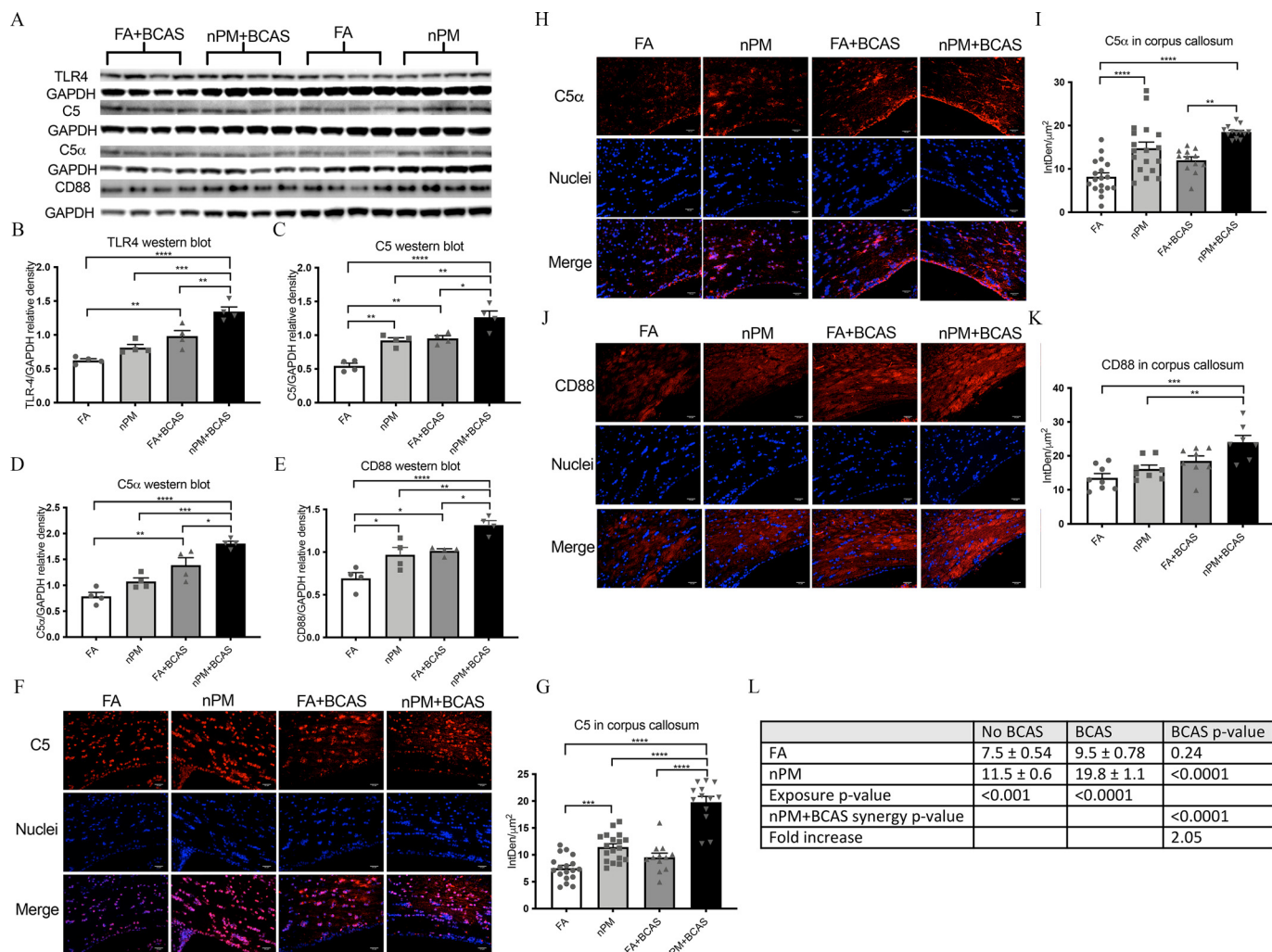
**Figure 4.** Measures of brain inflammation in the corpus callosum and whole brain of mice exposed to nPM or FA with or without BCAS. (A) Representative western blots of TLR4, C5, C5α, and CD88 (representative GAPDH blot) in the whole brain of mice in each experimental group. (B–E) TLR4, C5, C5α, and CD88 relative densities in the whole brain of mice in each experimental group. (F) Representative images of C5 (red) immunofluorescence and nuclei (blue) in the corpus callosum of mice in each experimental group (200×). (G) C5 immunofluorescent density in the corpus callosum of mice in each experimental group. (H) Representative images of C5α (red) immunofluorescence and nuclei (blue) in the corpus callosum of mice in each experimental group (200x). (I) C5α immunofluorescent density in the corpus callosum of mice in each experimental group. (J) Representative images of CD88 (red) immunofluorescence and nuclei (blue) in the corpus callosum of mice in each experimental group (200x). (K) CD88 immunofluorescent density in the corpus callosum of in each experimental group. (L) Effect of single and joint nPM and BCAS exposure on C5 immunofluorescent density in the corpus callosum of mice. General linear model with main effects for nPM, BCAS, nPM + BCAS interaction was used to calculate the synergy p-value. Exposure and BCAS *p*-values were calculated using the Tukey Kramer adjustment. Numbers are mean ± standard error. Analyses for F–K were performed on both right/left sides (right region demarcated area in Figure 2B). Data represented as mean ± standard error. Scale bars represent 50 μm. Error bars represent standard error. (A–E) $n = 4$ FA, 4 nPM, 4 FA + BCAS, 4 nPM + BCAS. (F–L) C5 and C5α: $n = 18$ FA, 18 nPM, 12 FA + BCAS, 13 nPM + BCAS; CD88: $n = 8$ FA, 8 nPM, 8 FA + BCAS, 7 nPM + BCAS. General linear model with main effects for nPM, BCAS, nPM + BCAS interaction were used; pairwise comparisons used Tukey Kramer adjustment. Summary data is provided in Table 1. Note: BCAS, bilateral carotid artery stenosis; C5, complement component 5; C5α, complement component 5α; CD88, complement component C5α receptor; FA, filtered air; nPM, nanoparticulate matter; TLR4, Toll-like receptor 4. $^{*}p < 0.05$, $^{**}p \leq 0.01$, $^{***}p \leq 0.001$, $^{****}p \leq 0.0001$.

FA + BCAS-exposed mice. The joint nPM + BCAS group mice had 124% higher 8-OHdG density when compared with the FA cohort ($7.6 \pm 0.3$ vs. $3.4 \pm 0.2$) but did not demonstrate a synergistic interaction with respect to 8-OHdG density (Table 1; Figure 5C,D).

### *Transcriptomic Responses (RNA-Seq)*

On transcriptomic response (RNA-Seq) analysis, differential expression was seen in Rnd3 [log2 fold change $-0.353$, $q = 0.0478$] and Pon2 [log2 fold change 0.193, $q = 0.048$] in the nPM exposure group when compared with FA controls (Table S8). Only one gene, Vps13c [log2 fold change $-0.283$, $q = 0.013$], demonstrated differential expression when BCAS

mice were compared with FA controls (Table S9). Fifty-four genes showed differential expression levels in the nPM + BCAS cohort when compared with FA controls (Table S10). Of these, only Ccl28 and Gm14827 were recurrent with single-exposure experiments, even when the stringency of the *q*-value was expanded to $\leq 0.10$. The expression of these genes followed a similar magnitude and direction of expression change as was seen in the single perturbation nPM group, with Ccl28 (log2 fold change 0.568, $q = 0.003$) and Gm14827 (log2 fold change $-0.498$, $q = 0.011$). There were no recurrent expression changes seen between the joint exposure group and the BCAS group. The heat map of these 54 genes demonstrated a distinct expression pattern in mice in the joint exposure group in comparison with nPM, with many genes being implicated in proinflammatory
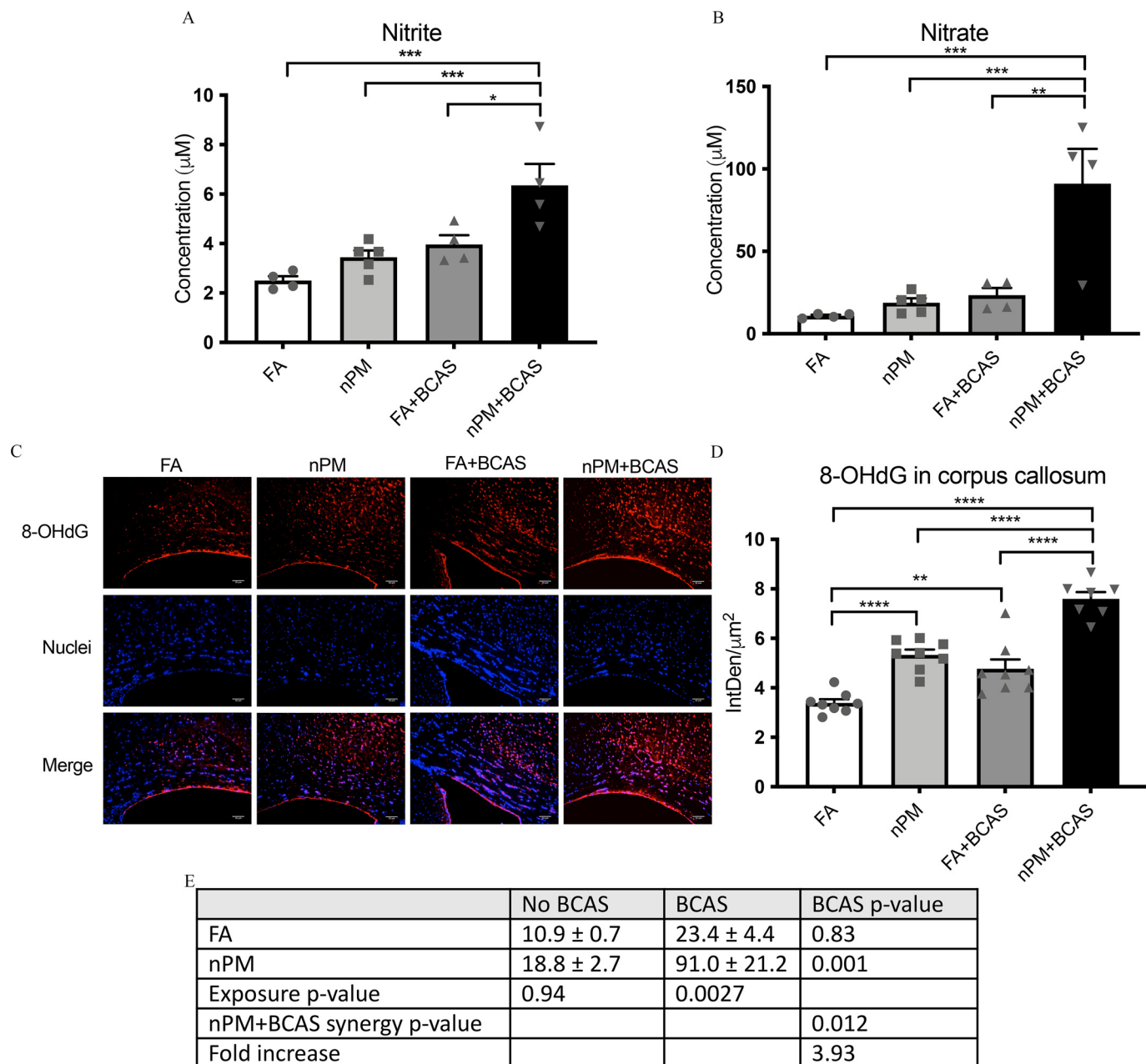
**Figure 5.** Measures of oxidative stress in the corpus callosum and whole brain of mice exposed to nPM or FA with or without BCAS. (A) Nitrite concentrations in the whole brain of mice in each experimental group. (B) Nitrate concentrations in the whole brain of mice in each experimental group. (C) Representative images of 8-OHdG (red) immunofluorescence and nuclei (blue) in the corpus callosum of mice in each experimental group (200×). Analysis was performed on both right/left sides (location of right region is demarcated area in Figure 2B). (D) 8-OHdG immunofluorescent density in the corpus callosum of mice in each experimental group. (E) Effect of single and joint nPM and BCAS exposure on nitrate concentrations in the whole brain of mice. General linear model with main effects for nPM, BCAS, nPM + BCAS interaction was used to calculate the synergy $p$-value. Exposure and BCAS $p$-values were calculated using the Tukey Kramer adjustment. Numbers are mean ± standard error. Data represented as mean ± standard error. Scale bars represent 50 µm. Error bars represent standard error. Nitrite and nitrate: $n = 4$ FA, 5 nPM, 4 FA + BCAS, 4 nPM + BCAS; 8-OHdG: $n = 8$ FA, 8 nPM, 8 FA + BCAS, 7 nPM + BCAS. General linear model with main effects for nPM, BCAS, and nPM + BCAS interaction were used; pairwise comparisons used Tukey Kramer adjustment. Summary data is provided in Table 1. Note: 8-OHdG, 8-oxo-2'-deoxyguanosine; BCAS, bilateral carotid artery stenosis; FA, filtered air; nPM, nanoscale particulate matter. $^{*}p < 0.05$, $^{**}p \leq 0.01$, $^{***}p \leq 0.001$, $^{****}p \leq 0.0001$.

pathways. The lack of generally recurrent expression patterns, along with the larger number of significant changes in the joint exposure group, suggested that a synergistic mechanism was responsible for changes (Figure 6). The genes listed in Tables S8, S9, and S10 were the only genes that were different among the exposure cohorts. A cohort of differentially expressed genes in RNA-Seq was validated by qPCR (Figure 6F; Table S11). qPCR results showed a similar direction and magnitude of response in comparison with those of transcriptomic responses (Figure 6F and Figure S3).

For Pathway Analysis, the filter was set to $q < 0.10$ (standard arbitrary value). All genes are reported in table format along with counts, $q$ and log2FoldChange values, and SE (Table S12). The nPM pollution network demonstrated activation of TNF (predicted) and CCL28 (observed), consistent with increased inflammation (Figure 6G). The BCAS hypoperfusion network
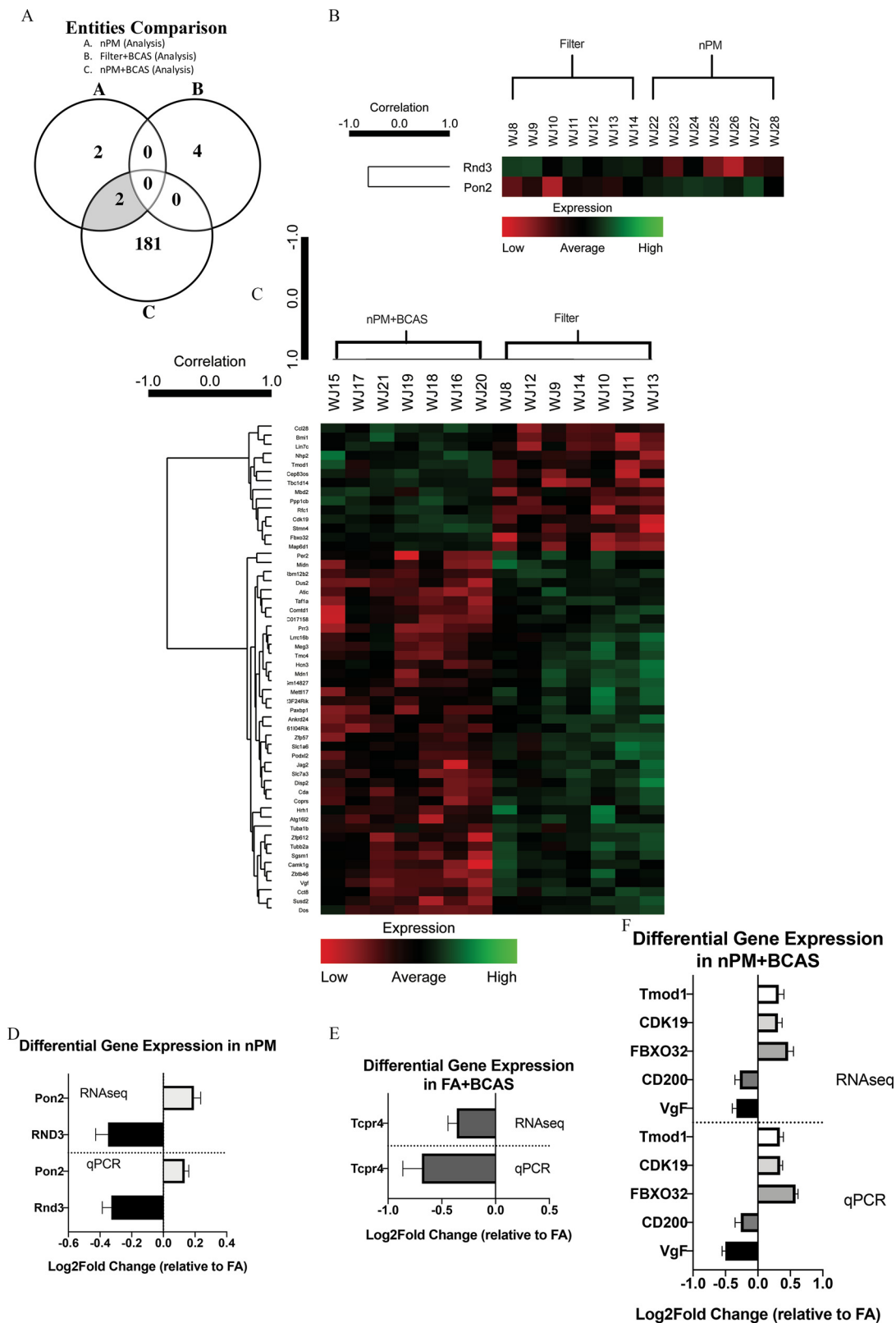
**Figure 6.** RNA-Seq and pathway analyses of mice exposed to nPM or FA with or without BCAS. (A–C) RNA-Seq analysis (Stringent false discovery rate $q < 0.05$). No heat map is included for FA vs. FA + BCAS because only one gene, VPS 13c, demonstrated differential expression. (A) Venn diagram of overlapping gene expression between nPM, FA + BCAS, and nPM + BCAS. (B) Heat map for differential gene expression for FA vs. nPM. (C) Heat map for differential gene expression for FA vs. nPM + BCAS. (D–F) qPCR validation of a subset of genes from RNA-Seq. GAPDH is used as a reference. Data represented as mean ± standard error. (G–J) Pathway analysis. (G) Pathway analysis for the nPM group (H) Pathway analysis for the BCAS group (I) Pathway analysis for the nPM + BCAS group. (J) Prediction legend. $n = 7$ FA, 7 nPM, 7 FA + BCAS, and 7 nPM + BCAS for qPCR and RNA-Seq analyses. Summary data is provided in Tables S8–S10, S12. qPCR summary data is provided in Table S11. Pathway analyses (G–J) were generated through the use of QIAGEN's Ingenuity Pathway Analysis (https://www.qiagenbioinformatics.com/products/ingenuitypathway-analysis; Krämer et al. 2014). Note: BCAS, bilateral carotid artery stenosis; FA, filtered air; nPM, nanoscale particulate matter; qPCR, quantitative real-time polymerase chain reaction; RNA-Seq, ribonucleic acid sequencing.
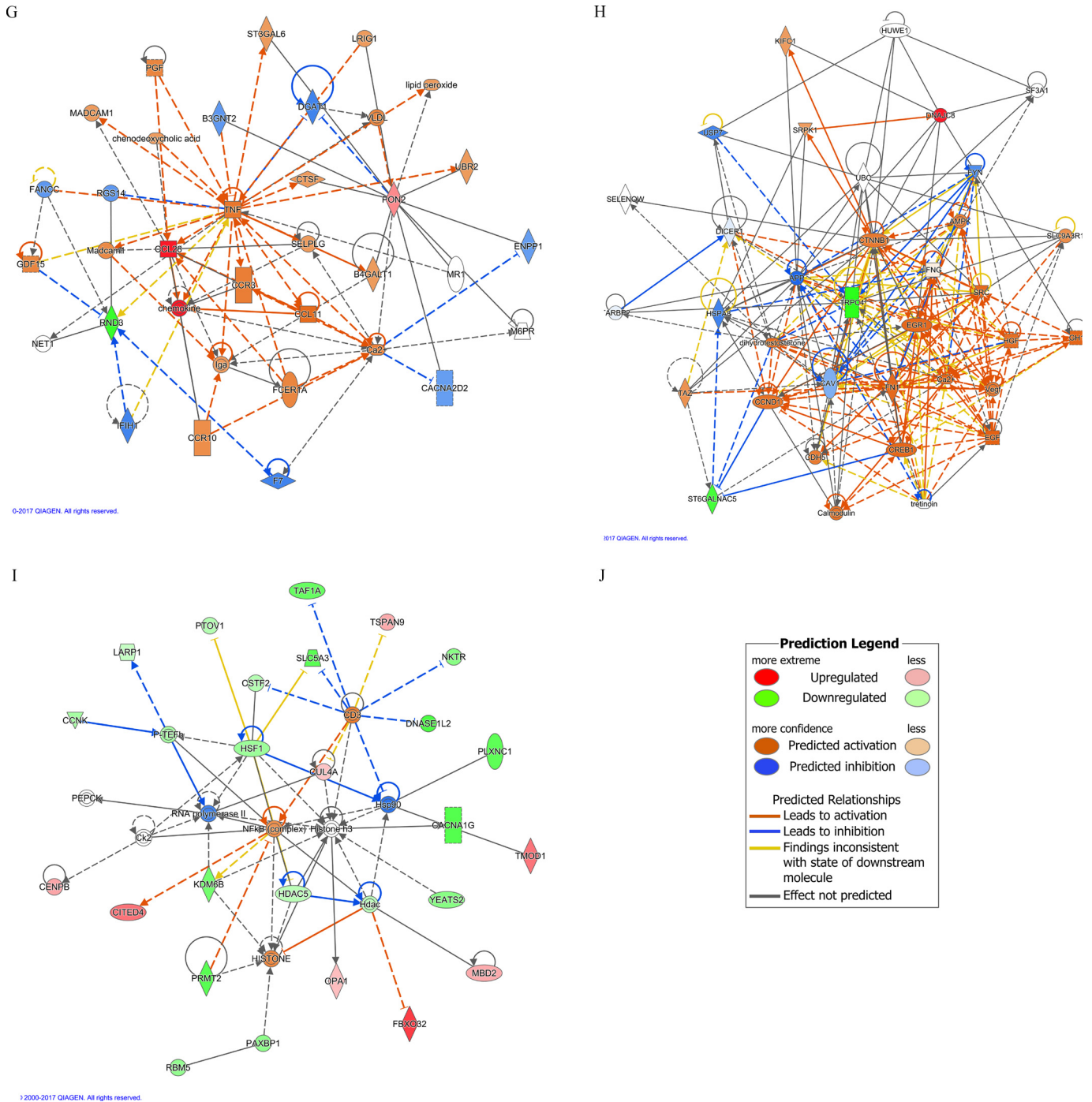
**Prediction Legend**

more extreme — less
- Upregulated
- Downregulated

more confidence — less
- Predicted activation
- Predicted inhibition

Predicted Relationships
— Leads to activation
— Leads to inhibition
— Findings inconsistent with state of downstream molecule
— Effect not predicted

**Figure 6.** (*Continued.*)

demonstrated downregulation of Trpc4 (observed) (Figure 6H). The combined pollution and hypoperfusion group network demonstrated a very "strong" pathway fit for network #2 (shown), with a high score and 25 molecules (observed). The network exhibited strong, central activation of NFKb, consistent with the proinflammatory milieu hypothesized (Figure 6I).

### Behavioral Deficits

Eight-arm radial maze testing data were analyzed using mixed effects models for repeatedly measured data. In a one-factor model comparing the four exposure groups, the groups significantly differed on revisiting errors: $F(3,44) = 2.84$, $p = 0.049$. In post hoc pairwise comparisons among the four groups adjusted for multiple comparisons, revisiting errors did not differ between the FA and nPM groups. However, nPM + BCAS-exposed mice had significantly more revisiting errors than the FA + BCAS-exposed mice ($8.8 \pm 0.4$ vs. $6.8 \pm 0.5$; $p = 0.04$). The joint nPM + BCAS group demonstrated 19% more mean revisiting errors across trials when compared with the filter cohort ($8.8 \pm 0.4$ vs. $7.4 \pm 1.4$). In a two-factor model ($\pm$ nPM exposure, $\pm$ BCAS), there was a significant main effect of nPM (assessed over $\pm$ BCAS groups), with more revisiting errors in nPM in comparison with FA groups ($p = 0.012$). The main effect of BCAS (assessed over $\pm$ nPM groups)

was not statistically significant. In another two-factor model treating trial as a continuous variable in the mixed model analysis, comparison of average slopes across trials approached significance for a synergistic interaction ($p = 0.064$). nPM-exposed mice in comparison with FA mice showed a significantly shallower slope of decreasing revisiting errors over trials ($p = 0.004$). The nPM + BCAS and FA + BCAS mice did not differ on slopes in revisiting errors. In the one-factor repeated measures comparison, the novel entry analysis showed a significant difference between the four exposure groups: $F(3,44) = 4.70$, $p = 0.006$. The joint nPM + BCAS group mice had 11% fewer novel entries across testing when compared with the FA cohort ($4.8 \pm 0.08$ vs. $5.4 \pm 0.3$). In the two-factor analysis, there was a significant main effect of nPM (over $\pm$ BCAS groups), with fewer novel entries in nPM in comparison with FA mice ($p = 0.005$); there was also a significant main effect of BCAS (over $\pm$ nPM groups), with fewer novel entries in BCAS compared with no-BCAS groups ($p = 0.034$). The analysis did not demonstrate a synergistic interaction when average slopes over trials were compared. Time course analysis showed significantly fewer revisiting errors [$F(7,318) = 23.98$, $p < 0.0001$] and more novel entries [$F(7,329) = 16.93$, $p < 0.0001$] within all groups, demonstrating learning effects of the testing (Table 1; Figure 7A–F).

In the NOR test, baseline behavior did not differ among groups. No mouse showed a preference for one identical object over the other. The discrimination index did not significantly differ between cohorts when mice explored two identical objects [$F(3,44) = 1.287$, $p = 0.29$]. In short-term NOR, the FA + BCAS cohort had a significantly lower discrimination index in comparison with the FA group. These interactions were not synergistic between groups. In long-term NOR, there was no significant difference between groups and no synergy (Table 1; Figure 7G,H).

## Discussion

Our experimental data demonstrated synergistic effects of nPM and CCH on white matter injury such that the joint influence was greater than the additive properties of the two independent exposures. Based on the primary outcome, KB staining, nPM + BCAS exhibited a synergistic interaction with regard to white matter injury scores in the corpus callosum ($p = 0.018$ for synergy). At the structural level, a higher level of myelin degradation in the nPM + BCAS cohort (in comparison with each of the other groups) was confirmed by dMBP histochemistry. Myelin integrity was also compromised in the single-exposure (nPM or FA + BCAS) cohorts when compared with the FA group. The significant difference noted between the FA and nPM cohorts on this histochemical analysis (which was not found to be different on the KB staining) likely resulted from the quantitative method used to analyze structural integrity at the cellular level (dMBP staining). The KB grading scale is a gross pathological assessment that evaluates the regional/global appearance of the corpus callosum.

White matter rarefaction in the joint exposure cohort was further documented on T2 weighted MRI, which demonstrated significantly smaller corpus callosum volumes when compared with mice in FA- or single-exposure groups. These data are reinforced by findings in experimental models of early postnatal exposure to concentrated ultrafine ambient particles. The studies revealed reduced corpus callosum sizes/developmental trajectories and lower myelination following exposure (Allen et al. 2017). PM effects on white matter volume, and possible moderating influences of cerebrovascular disease (CVD), were also suggested in epidemiological studies. In an analysis of the Women's Health Initiative Memory Study (WHIMS) cohort, older women who resided in areas with greater long-term $PM_{2.5}$ exposure had significantly smaller white matter volumes in the corpus callosum and frontal/temporal lobes but unchanged gray matter volumes (Chen et al. 2015). Stronger associations in older women with prior CVD suggested possible interactions of CVD-related neurovascular injury (Chen et al. 2015) and the underlying neuropathological processes resulting in white matter loss associated with $PM_{2.5}$ neurotoxicity.

When intact, the BBB effectively restricts vascular access to most brain regions, protecting tissue from systemic toxins (Miller 2010). White matter injury was documented in experimental models of impaired BBB permeability. In a pericyte-deficient ($Pdgfrb^{F7/F7}$) mouse model, pericyte degeneration impaired the white matter microcirculation. These changes resulted in accumulation of toxic blood-derived products and reduced regional cerebral blood flow, leading to loss of white matter constituents (myelin, axons, and oligodendrocytes) and corresponding functional deficits (Montagne et al. 2018). Our previous study demonstrated increased BBB leakage due to lower pericyte coverage in the mouse BCAS model (Liu et al. 2019). BBB permeability increased on postoperative day 1, peaked at day 3, and stabilized to nearly baseline levels by day 30. Large molecules, such as IgG (approximately 150 KD), leaked into the perivascular space at day 3 and then persisted in the tissue. BBB permeability changes occurred significantly earlier than structural white matter injury (day 30) in the same anatomical regions and white matter tracts. Transient BBB permeability may allow penetration of inflammatory mediators and byproducts of oxidative stress, generated by nPM exposure (and CCH), into the cortical white matter.

A previous study using a murine model established that neuroinflammation plays a central role in PM-induced CNS injury and that microglial activation is a critical mediator of these processes (Peters et al. 2006). One of our prior studies demonstrated that mice exhibited reactive microglia and higher deposition of complement C5 protein and its C5a receptor 1 (CD88) in the corpus callosum following 10 wk of nPM exposure (Babadjouni et al. 2018). In the current study, BCAS and nPM exposure resulted in higher glial cell activation in the corpus callosum of mice. CNS myeloid cells, such as microglia, were selectively activated by both the individual nPM and CCH exposures, whereas reactive astrocytes were noted only in the setting of CCH (no additive increase from nPM). This microglial-specific activation in the corpus callosum is consistent with our prior nPM study (Babadjouni et al. 2018).

Western blot (whole brain) and histochemical analyses (corpus callosum) demonstrated that nPM + BCAS exposure resulted in higher degrees of inflammation in the whole brain and corpus callosum, with synergistic effects on C5 deposition in the corpus callosum. Higher levels of TLR4 protein was also noted in the whole brain tissue of the joint nPM + BCAS group. A prior study suggested that TLR4 activation was integral in the brain inflammatory responses to air pollution (Woodward et al. 2017a). *In vivo* nPM exposure of mice induced TLR4 and downstream genes in the hippocampus (Woodward et al. 2017a). Further, TLR4 knockdown in mixed glial cultures attenuated the neuroinflammatory response to nPM (Woodward et al. 2017a). These findings suggest a potential microglia-mediated inflammatory response that may involve the TLR4 and complement pathways (C5 component). As each is a constituent of the innate immune response, functional interplay between TLRs and C5 activation has been described (DiMartino et al. 2008; Hajishengallis and Lambris 2010; Raby et al. 2011). C5a receptor activation has been indicated to up-regulate TLR4-mediated TNFα production in the absence of decay accelerating factor in mice (Zhang et al. 2007). Previous studies have demonstrated that ultrafine PM
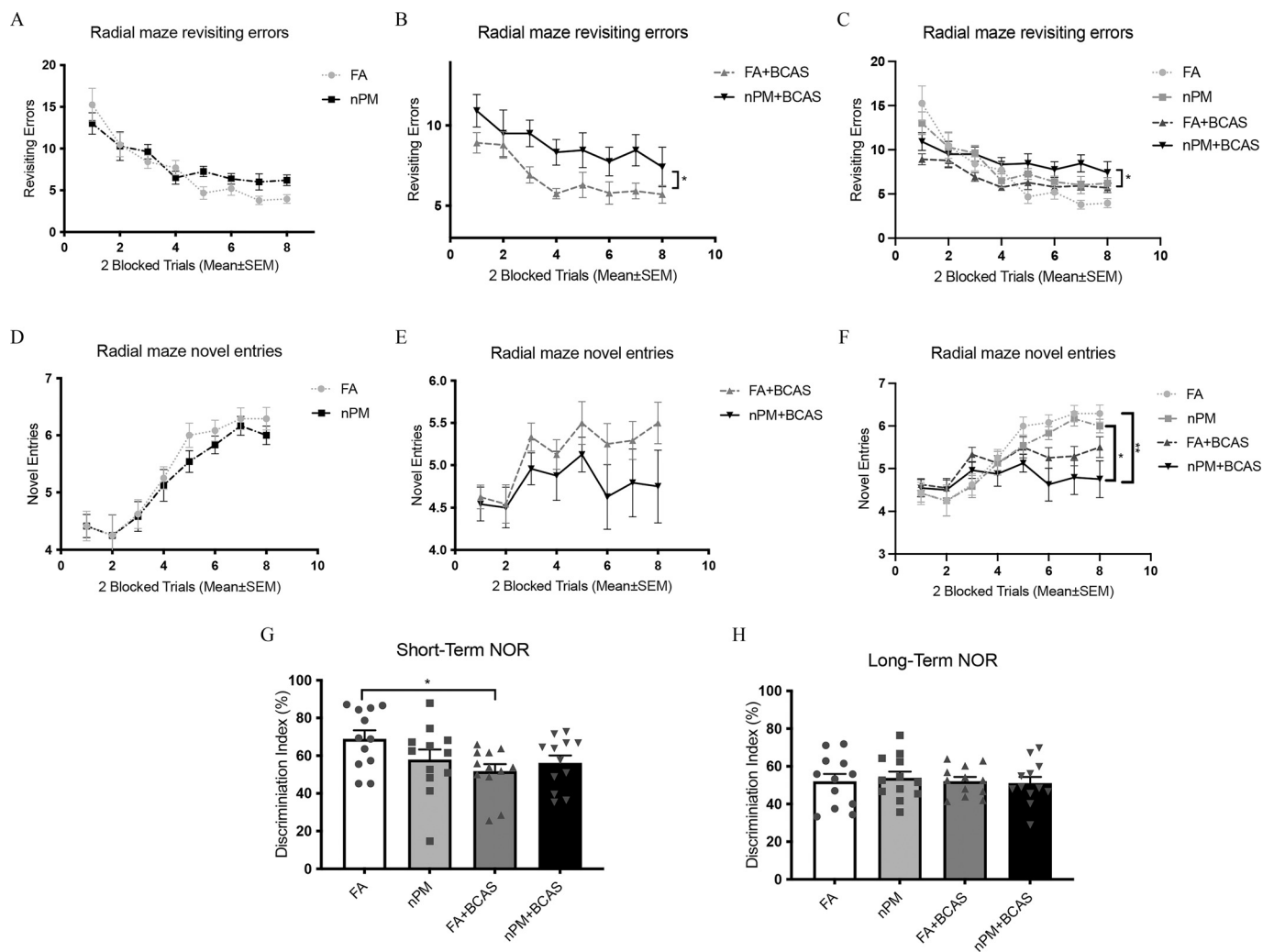
**Figure 7.** Behavioral analyses of mice exposed to nPM or FA with or without BCAS. (A–C) Radial maze revisiting errors in mice exposed to nPM or FA with or without BCAS. (D–F) Radial maze novel entries in mice exposed to nPM or FA with or without BCAS. (G) Short-term NOR discrimination index in mice exposed to nPM or FA with or without BCAS. (H) Long-term NOR discrimination index in mice exposed to nPM or FA with or without BCAS. Data represented as mean $\pm$ standard error. $n = 12$ FA, 12 nPM, 12 FA + BCAS, 12 nPM + BCAS. (A–F) General linear model with main effects for nPM, BCAS, nPM + BCAS interaction were used; pairwise comparisons used Tukey Kramer adjustment. (E–F) For the 8-arm radial maze, a mixed effects repeated measures model (8 averaged blocked trial) was used to analyze: differences among the four groups (one-factor model), and main effects for nPM, BCAS and the nPM + BCAS interaction (two-factor model). Mean slope (behavior outcome over trials) was analyzed using a linear mixed effects model with main effects for nPM, BCAS, and the nPM + BCAS interaction, modeling trial as a continuous variable. Summary data is provided in Table 1. Note: BCAS, bilateral carotid artery stenosis; FA, filtered air; NOR, novel object recognition; nPM, nanoscale particulate matter. $^*p < 0.05$, $^{**}p \leq 0.01$, $^{***}p \leq 0.001$, $^{****}p \leq 0.0001$.

activates microglia and induces TNFα production, which in turn inhibits neurite outgrowth (Babadjouni et al. 2018; Cheng et al. 2016).

Corpus callosum RNA response data confirmed the joint influence of nPM and CCH to be greater than the additive effects of each exposure at the gene/RNA level. Further, the experiments supported a critical role for neuroinflammation. Differential gene expression between the FA and joint exposure (nPM + BCAS) paradigms demonstrated a greater gene response than did the nPM or FA + BCAS cohorts alone (when compared with the FA cohort). In pathway analysis, the nPM network suggested activation of CCL28 (observed) and TNF (predicted), supporting potential inflammatory mechanisms. The CCH network demonstrated down-regulation of Trpc4 , which may play a role in endothelial permeability and/or vasodilation. Trpc4 is principally found in endothelial cells, vascular smooth muscle cells, and mast cells. Members of the TRP family recognize LPS and have been proposed as chemosensors involved in toxin detection

(Dietrich et al. 2017). The joint nPM/CCH pathway analysis suggested strong, central activation of NFkB, once again indicating a strong inflammatory milieu and supporting a potential upstream role for TLR4. A previous study demonstrated strong *in vitro* glial activation of both TLR4 and NFkB in response to nanoscale PM (Woodward et al. 2017a).

Traffic-related air pollution caused oxidative stress in rodent models (Cheng et al. 2016; Haghani et al. 2020; Morgan et al. 2011). Moreover, nPM promoted lipid raft alterations that resulted in higher production of the neurotoxic amyloid peptide Aβ *in vitro* and *in vivo* (Cacciottolo et al. 2020). Following ischemic stroke, nPM-exposed mice demonstrated higher levels of oxidative stress markers (8-hydroxyguanosine) and reactive oxygen species (gp91[phox]) in the region of the ischemic penumbra (Babadjouni et al. 2018). Concordant with these findings, the joint nPM + BCAS group in the present study demonstrated higher levels of nitrite/nitrate in the whole brain and 8-OHdG in the corpus callosum when compared with each of the other

exposure groups. nPM + BCAS exposure resulted in synergistic effects on whole brain nitrate concentrations.

No overt working memory deficits were noted on 8-arm radial maze testing following 10 wk of nPM exposure alone. However, the nPM + BCAS-exposed mice exhibited a significantly higher degree of neurocognitive injury than did the FA + BCAS-exposed mice. Further, changes in the slope of revisiting errors across blocked trials approached statistical significance for synergism in the nPM + BCAS group. The enhanced behavioral deficits (8-arm radial maze testing) exhibited by our joint exposure group were relatively specific to spatial working memory. Similar changes were not evident in NOR testing. Both 8-arm radial maze (Shibata et al. 2007) and NOR testing (Patel et al. 2017) previously yielded reproducible deficits in the murine BCAS model. This is the reason for choosing these outcome measures in this joint exposure study. The current data suggested that the addition of the nPM exposure selectively augmented the deleterious effects on spatial working memory (8-arm radial maze). Working memory impairment, as assessed by the 8-arm radial maze, may be attributable to either frontal white matter lesions or hippocampal injury. The correlative pathology in prior BCAS studies suggested white matter tract injury (Liu et al. 2013; Patel et al. 2017; Shibata et al. 2004). In contrast, NOR testing is a classic assessment of recognition memory (a subtype of declarative memory) and typically used to study hippocampal function. Deficits in recognition memory (NOR testing) in the murine BCAS model likely resulted from involvement of the perirhinal cortex, communicating white matter tracts, or hippocampus (Patel et al. 2017). Prior studies confirmed that white matter damage was more robust than hippocampal injury following murine BCAS with 0.018 mm inner diameter microcoils (as employed in this study) (Patel et al. 2017; Shibata et al. 2004). The white matter damage and resultant behavioral deficits noted in these exposures correlated with clinical pathology.

There are inherent limitations to these studies. Our cohort consisted of exclusively male mice. Prior studies suggest that estrogen may exhibit a protective effect on white matter injury (Gerstner et al. 2009; Allen et al. 2017; Dominguez et al. 2018). Our previous data demonstrated that estrogen impacted susceptibility to experimental CCH in this model. Following BCAS, male mice treated with oral 17β-estradiol demonstrated less white matter ischemic damage and neurocognitive deficits (NOR) than did placebo treated mice (Dominguez et al. 2018). The numbers of mice were limited by the exposure paradigm and did not allow inclusion of sex or age as a third variable to nPM and BCAS. Because the current study established the synergistic effects of nPM and CCH in young male mice, future studies can assess the impact of sex and age differences on these exposures and outcomes. Control (nonoperated), rather than sham-operated mice, were chosen, *a priori*, for the FA and nPM groups so that the nPM effects on white matter injury, inflammatory biomarkers, and, particularly, behavior could be evaluated in the absence of a surgical procedure. These outcomes had not previously been examined and, as expected, were subtle. The effects of the surgical procedure (in addition to CCH), manifested equally in the FA + BCAS and nPM + BCAS cohorts. Tests for synergy are typically low in statistical power (Turner et al. 2014). Sample size limitations may have affected end point analyses that appeared to display additive joint exposure effects but did not reach statistical significance for synergy. It is known that behavior testing protocols (behavior testing/food deprivation) can modify the brain and influence outcomes (Rosenzweig and Bennett 1996; Squadrito et al. 1994). Our results found no significant differences in white matter injury or neuroinflammatory markers between mice that underwent behavioral testing and mice that did not.

Exposure system characteristics present as both strengths and limitations. Strengths include small particle size with a composition that retains the chemical properties of traffic-related air pollution. The average particle size distribution of the exposure aerosol (Figure S1) was typical of PM in the Los Angeles air basin, an urban area affected by traffic emissions (Hudda et al. 2010; Taghvaee et al. 2019). The current setup minimized the within-exposure variability, an advantage over other systems such as particle concentrators.

The differences between exposures were a reflection of the natural variability of the Los Angeles aerosol, because the particles used in these exposures were generated by aerosolizing suspensions of "real-world" particles collected during several weeks across different seasons and years in central Los Angeles. The reported ranges in the OC and metal mass fractions were consistent with our earlier studies (greater than 20 y) in the Los Angeles basin (Altuwayjiri et al. 2021; Hasheminassab et al. 2014b; Saffari et al. 2013; Sardar et al. 2005; Shirmohammadi et al. 2016).

Limitations include the fact that the resuspended particles may not retain the same surface chemistry or shape of the original particles and that this approach used a concentration which is likely one to two orders of magnitude larger than the ultrafine exposures that people experience. The bulk composition and size distribution of the resuspended particles were similar to the original exposure aerosol.

The mass-based exposure levels ($305.6 \pm 11.7\,\mu g/m^3$) were roughly one order of magnitude higher than those typical of central Los Angeles, which were in the range of $25$–$35\,\mu g/m^3$ (Hasheminassab et al. 2014a). These were, however, subacute exposures compared with the urban background concentration of Los Angeles. These PM mass levels have been noted in cities of the developing world, such as Beijing, New Delhi, Lagos, Cairo, Mexico City, etc. (Jimenez et al. 2009). The number-based concentration levels were twice as high as those at Los Angeles freeways or in the proximity of the Los Angeles International (LAX) airport but not unrealistic in terms of human exposure (Shirmohammadi et al. 2017).

Direct comparison of the exposure levels between two different species are facilitated by taking into account anatomical and physiological differences. Dose per kilogram of body weight measurements are used in conventional pharmacokinetics to calculate the toxicity or carcinogenicity of a substance. In that regard, the exposure concentration level of roughly $330\,\mu g/m^3$ for mice represented a realistic exposure level for humans. During this exposure period, the PM concentration that would have resulted in the same PM dose per kilogram body weight is $PM_{2.5} = 33\,\mu g/m^3$. This is a very realistic PM exposure level, typical of $PM_{2.5}$ concentrations in Los Angeles, as well as in other urban areas in California (Hasheminassab et al. 2014b).

These data demonstrated synergistic effects of nPM exposure and CCH secondary to carotid stenosis with respect to white matter injury. Increased BBB permeability secondary to CCH may permit greater entry of proinflammatory mediators and byproducts of oxidative stress into the cortical white matter (corpus callosum). Similarly, the deleterious effects of PM exposure may exacerbate ischemic injury from cerebral hypoperfusion. These two exposures likely influence each other in a reciprocated fashion, with each compounding the effects of the other. To the best of our knowledge, this study provides the first, and strong, experimental evidence that air pollution can have greater neurotoxicity on vulnerable populations such as those with underlying cerebrovascular disease. These findings could have implications for individuals with cerebral hypoperfusion from carotid stenosis, intracranial atherosclerosis, or cerebral small vessel disease. Such

experimental data provide the neurobiological basis to better understand the increased susceptibility to environmental neurotoxicity that may help explain disparities in brain health at the population level and ultimately aid with risk-factor stratification.

## Acknowledgments

## References

Allen JL, Oberdorster G, Morris-Schaffer K, Wong C, Klocke C, Sobolewski M, et al. 2017. Developmental neurotoxicity of inhaled ambient ultrafine particle air pollution: parallels with neuropathological and behavioral features of autism and other neurodevelopmental disorders. Neurotoxicology 59:140–154, PMID: 26721665, https://doi.org/10.1016/j.neuro.2015.12.014.

Altuwayjiri A, Pirhadi M, Taghvaee S, Sioutas C. 2021. Long-term trends in the contribution of pm(2.5) sources to organic carbon (OC) in the Los Angeles basin and the effect of PM emission regulations. Faraday Discuss 226:74–99, PMID: 33241815, https://doi.org/10.1039/D0FD00074D.

Babadjouni R, Patel A, Liu Q, Shkirkova K, Lamorie-Foote K, Connor M, et al. 2018. Nanoparticulate matter exposure results in neuroinflammatory changes in the corpus callosum. PLoS One 13(11):e0206934, PMID: 30395590, https://doi.org/10.1371/journal.pone.0206934.

Benedictus MR, Binnewijzend MAA, Kuijer JPA, Steenwijk MD, Versteeg A, Vrenken H, et al. 2014. Brain volume and white matter hyperintensities as determinants of cerebral blood flow in Alzheimer's disease. Neurobiology of Aging 35(12):2665–2670, PMID: 25018106, https://doi.org/10.1016/j.neurobiolaging.2014.06.001.

Bevins RA, Besheer J. 2006. Object recognition in rats and mice: a one-trial non-matching-to-sample learning task to study 'recognition memory'. Nat Protoc 1(3):1306–1311, PMID: 17406415, https://doi.org/10.1038/nprot.2006.205.

Biran R, Tang Y-Z, Brook JR, Vincent R, Keeler GJ. 1996. Aqueous extraction of airborne particulate matter collected on hi-vol Teflon filters. International Journal of Environmental Analytical Chemistry 63(4):315–322, https://doi.org/10.1080/03067319608028327.

Block ML, Elder A, Auten RL, Bilbo SD, Chen H, Chen JC, et al. 2012. The outdoor air pollution and brain health workshop. Neurotoxicology 33(5):972–984, PMID: 22981845, https://doi.org/10.1016/j.neuro.2012.08.014.

Bos I, De Boever P, Emmerechts J, Buekers J, Vanoirbeek J, Meeusen R, et al. 2012. Changed gene expression in brains of mice exposed to traffic in a highway tunnel. Inhal Toxicol 24(10):676–686, PMID: 22906174, https://doi.org/10.3109/08958378.2012.714004.

Cacciottolo M, Morgan TE, Saffari AA, Shirmohammadi F, Forman HJ, Sioutas C, et al. 2020. Traffic-related air pollutants (trap-pm) promote neuronal amyloidogenesis through oxidative damage to lipid rafts. Free Radic Biol Med 147:242–251, PMID: 31883973, https://doi.org/10.1016/j.freeradbiomed.2019.12.023.

Cacciottolo M, Wang X, Driscoll I, Woodward N, Saffari A, Reyes J, et al. 2017. Particulate air pollutants, APOE alleles and their contributions to cognitive impairment in older women and to amyloidogenesis in experimental models. Transl Psychiatry 7(1):e1022, PMID: 28140404, https://doi.org/10.1038/tp.2016.280.

Campbell A, Oldham M, Becaria A, Bondy SC, Meacher D, Sioutas C, et al. 2005. Particulate matter in polluted air may increase biomarkers of inflammation in mouse brain. Neurotoxicology 26(1):133–140, PMID: 15527881, https://doi.org/10.1016/j.neuro.2004.08.003.

Chen JC, Wang X, Wellenius GA, Serre ML, Driscoll I, Casanova R, et al. 2015. Ambient air pollution and neurotoxicity on brain structure: evidence from women's health initiative memory study. Ann Neurol 78(3):466–476, PMID: 26075655, https://doi.org/10.1002/ana.24460.

Cheng Y, Pardo M, Armini RS, Martinez A, Mouhsine H, Zagury JF, et al. 2016. Stress-induced neuroinflammation is mediated by GSK3-dependent TLR4 signaling that promotes susceptibility to depression-like behavior. Brain Behav Immun 53:207–222, PMID: 26772151, https://doi.org/10.1016/j.bbi.2015.12.012.

Choi BR, Kim DH, Back DB, Kang CH, Moon WJ, Han JS, et al. 2016. Characterization of white matter injury in a rat model of chronic cerebral hypoperfusion. Stroke 47(2):542–547, PMID: 26670084, https://doi.org/10.1161/STROKEAHA.115.011679.

Crane DE, Black SE, Ganda A, Mikulis DJ, Nestor SM, Donahue MJ, et al. 2015. Gray matter blood flow and volume are reduced in association with white matter hyperintensity lesion burden: a cross-sectional MRI study. Front Aging Neurosci 7:131, PMID: 26217223.

de la Torre JC. 2004. Alzheimer's disease is a vasocognopathy: a new term to describe its nature. Neurol Res 26(5):517–524, PMID: 15265269, https://doi.org/10.1179/016164104225016254.

Dietrich A, Steinritz D, Gudermann T. 2017. Transient receptor potential (TRP) channels as molecular targets in lung toxicology and associated diseases. Cell Calcium 67:123–137, PMID: 28499580, https://doi.org/10.1016/j.ceca.2017.04.005.

DiMartino SJ, Yuan W, Redecha P, Ivashkiv LB, Salmon JE. 2008. Insoluble immune complexes are most effective at triggering IL-10 production in human monocytes and synergize with TLR ligands and C5a. Clin Immunol 127(1):56–65, PMID: 18201931, https://doi.org/10.1016/j.clim.2007.11.014.

Dominguez R, Zitting M, Liu Q, Patel A, Babadjouni R, Hodis DM, et al. 2018. Estradiol protects white matter of male C57BL6J mice against experimental chronic cerebral hypoperfusion. J Stroke Cerebrovasc Dis 27(7):1743–1751, PMID: 29602614, https://doi.org/10.1016/j.jstrokecerebrovasdis.2018.01.030.

Emrani S, Libon DJ, Lamar M, Price CC, Jefferson AL, Gifford KA, et al. 2018. Assessing working memory in mild cognitive impairment with serial order recall. J Alzheimers Dis 61(3):917–928, PMID: 29254087, https://doi.org/10.3233/JAD-170555.

Ennaceur A, Delacour J. 1988. A new one-trial test for neurobiological studies of memory in rats. 1: behavioral data. Behav Brain Res 31(1):47–59, PMID: 3228475, https://doi.org/10.1016/0166-4328(88)90157-x.

Erickson LD, Gale SD, Anderson JE, Brown BL, Hedges DW. 2020. Association between exposure to air pollution and total gray matter and total white matter volumes in adults: a cross-sectional study. Brain Sci 10:, PMID: 32182984, https://doi.org/10.3390/brainsci10030164.

Forman HJ, Finch CE. 2018. A critical review of assays for hazardous components of air pollution. Free Radic Biol Med 117:202–217, PMID: 29407794, https://doi.org/10.1016/j.freeradbiomed.2018.01.030.

Gerstner B, Lee J, DeSilva TM, Jensen FE, Volpe JJ, Rosenberg PA. 2009. 17beta-estradiol protects against hypoxic/ischemic white matter damage in the neonatal rat brain. J Neurosci Res 87(9):2078–2086, PMID: 19224575, https://doi.org/10.1002/jnr.22023.

Haghani A, Cacciottolo M, Doty KR, D'Agostino C, Thorwald M, Safi N, et al. 2020. Mouse brain transcriptome responses to inhaled nanoparticulate matter differed by sex and APOE in NRF2-NFKb interactions. elife 9:, PMID: 32579111, https://doi.org/10.7554/eLife.54822.

Hajishengallis G, Lambris JD. 2010. Crosstalk pathways between toll-like receptors and the complement system. Trends Immunol 31(4):154–163, PMID: 20153254, https://doi.org/10.1016/j.it.2010.01.002.

Hasheminassab S, Daher N, Ostro BD, Sioutas C. 2014a. Long-term source apportionment of ambient fine particulate matter (PM2.5) in the Los Angeles Basin: a focus on emissions reduction from vehicular sources. Environ Pollut 193:54–64, PMID: 25005887, https://doi.org/10.1016/j.envpol.2014.06.012.

Hasheminassab S, Daher N, Saffari A, Wang D, Ostro BD, Sioutas C. 2014b. Spatial and temporal variability of sources of ambient fine particulate matter (pm$_{2.5}$) in California. Atmos Chem Phys 14(22):12085–12097, https://doi.org/10.5194/acp-14-12085-2014.

Herner JD, Green PG, Kleeman MJ. 2006. Measuring the trace elemental composition of size-resolved airborne particles. Environ Sci Technol 40(6):1925–1933, PMID: 16570617, https://doi.org/10.1021/es052315q.

Hudda N, Cheung K, Moore KF, Sioutas C. 2010. Inter-community variability in total particle number concentrations in the eastern Los Angeles air basin. Atmos Chem Phys 10(23):11385–11399, https://doi.org/10.5194/acp-10-11385-2010.

Jimenez JL, Canagaratna MR, Donahue NM, Prevot AS, Zhang Q, Kroll JH, et al. 2009. Evolution of organic aerosols in the atmosphere. Science 326(5959):1525–1529, PMID: 20007897, https://doi.org/10.1126/science.1180353.

Kim CM, Alvarado RL, Stephens K, Wey HY, Wang DJJ, Leritz EC, et al. 2020. Associations between cerebral blood flow and structural and functional brain

imaging measures in individuals with neuropsychologically defined cognitive impairment. Neurobiol Aging 86:64–74, PMID: 31813626, https://doi.org/10.1016/j.neurobiolaging.2019.10.023.

Krämer A, Green J, Pollard J Jr, Tugendreich S. 2014. Causal analysis approaches in Ingenuity Pathway Analysis. Bioinformatics. 30(4):523–530, PMID: 24336805, https://doi.org/10.1093/bioinformatics/btt703.

Kulick ER, Elkind MSV, Boehme AK, Joyce NR, Schupf N, Kaufman JD, et al. 2020. Long-term exposure to ambient air pollution, APOE-ε4 status, and cognitive decline in a cohort of older adults in northern Manhattan. Environ Int 136:105440, PMID: 31926436, https://doi.org/10.1016/j.envint.2019.105440.

Liu Q, He S, Groysman L, Shaked D, Russin J, Scotton TC, et al. 2013. White matter injury due to experimental chronic cerebral hypoperfusion is associated with C5 deposition. PLoS One 8(12):e84802, PMID: 24386419, https://doi.org/10.1371/journal.pone.0084802.

Liu Q, Radwanski R, Babadjouni R, Patel A, Hodis DM, Baumbacher P, et al. 2019. Experimental chronic cerebral hypoperfusion results in decreased pericyte coverage and increased blood-brain barrier permeability in the corpus callosum. J Cereb Blood Flow Metab 39(2):240–250, PMID: 29192539, https://doi.org/10.1177/0271678X17743670.

Lough GC, Schauer JJ, Park JS, Shafer MM, Deminter JT, Weinstein JP. 2005. Emissions of metals associated with motor vehicle roadways. Environ Sci Technol 39(3):826–836, PMID: 15757346, https://doi.org/10.1021/es048715f.

Mauderly JL, Samet JM. 2009. Is there evidence for synergy among air pollutants in causing health effects? Environ Health Perspect 117(1):1–6, PMID: 19165380, https://doi.org/10.1289/ehp.11654.

Miller DS. 2010. Regulation of p-glycoprotein and other ABC drug transporters at the blood-brain barrier. Trends in Pharmacological Sciences 31(6):246–254, PMID: 20417575, https://doi.org/10.1016/j.tips.2010.03.003.

Misra C, Kim S, Shen S, Sioutas C. 2002. A high flow rate, very low pressure drop impactor for inertial separation of ultrafine from accumulation mode particles. Journal of Aerosol Science 33(5):735–752, https://doi.org/10.1016/S0021-8502(01)00210-5.

Montagne A, Nikolakopoulou AM, Zhao Z, Sagare AP, Si G, Lazic D, et al. 2018. Pericyte degeneration causes white matter dysfunction in the mouse central nervous system. Nat Med 24(3):326–337, PMID: 29400711, https://doi.org/10.1038/nm.4482.

Morgan TE, Davis DA, Iwata N, Tanner JA, Snyder D, Ning Z, et al. 2011. Glutamatergic neurons in rodent models respond to nanoscale particulate urban air pollutants in vivo and in vitro. Environ Health Perspect 119(7):1003–1009, PMID: 21724521, https://doi.org/10.1289/ehp.1002973.

Patel A, Moalem A, Cheng H, Babadjouni RM, Patel K, Hodis DM, et al. 2017. Chronic cerebral hypoperfusion induced by bilateral carotid artery stenosis causes selective recognition impairment in adult mice. Neurol Res 39(10):910–917, PMID: 28828966, https://doi.org/10.1080/01616412.2017.1355423.

Peters R, Ee N, Peters J, Booth A, Mudway I, Anstey KJ. 2019. Air pollution and dementia: a systematic review. J Alzheimers Dis 70(S1):S145–S163, PMID: 30775976, https://doi.org/10.3233/JAD-180631.

Peters A, Veronesi B, Calderón-Garcidueñas L, Gehr P, Chen LC, Geiser M, et al. 2006. Translocation and potential neurological effects of fine and ultrafine particles a critical update. Part Fibre Toxicol 3:13, PMID: 16961926, https://doi.org/10.1186/1743-8977-3-13.

Petkus AJ, Younan D, Widaman K, Gatz M, Manson JE, Wang X, et al. 2020. Exposure to fine particulate matter and temporal dynamics of episodic memory and depressive symptoms in older women. Environ Int 135:105196, PMID: 31881430, https://doi.org/10.1016/j.envint.2019.105196.

Raby AC, Holst B, Davies J, Colmont C, Laumonnier Y, Coles B, et al. 2011. TLR activation enhances C5a-induced pro-inflammatory responses by negatively modulating the second C5a receptor, C5L2. Eur J Immunol 41(9):2741–2752, PMID: 21630250, https://doi.org/10.1002/eji.201041350.

Rosenzweig MR, Bennett EL. 1996. Psychobiology of plasticity: effects of training and experience on brain and behavior. Behav Brain Res 78(1):57–65, PMID: 8793038, https://doi.org/10.1016/0166-4328(95)00216-2.

Saffari A, Daher N, Shafer MM, Schauer JJ, Sioutas C. 2013. Seasonal and spatial variation of trace elements and metals in quasi-ultrafine (PM$_{0.25}$) particles in the Los Angeles metropolitan area and characterization of their sources. Environ Pollut 181:14–23, PMID: 23800424, https://doi.org/10.1016/j.envpol.2013.06.001.

Sardar SB, Fine PM, Sioutas C. 2005. Seasonal and spatial variability of the size-resolved chemical composition of particulate matter (PM10) in the Los Angeles basin. J Geophys Res 110(D7):, https://doi.org/10.1029/2004JD004627.

Shibata M, Ohtani R, Ihara M, Tomimoto H. 2004. White matter lesions and glial activation in a novel mouse model of chronic cerebral hypoperfusion. Stroke

35(11):2598–2603, PMID: 15472111, https://doi.org/10.1161/01.STR.0000143725.19053.60.

Shibata M, Yamasaki N, Miyakawa T, Kalaria RN, Fujita Y, Ohtani R, et al. 2007. Selective impairment of working memory in a mouse model of chronic cerebral hypoperfusion. Stroke 38(10):2826–2832, PMID: 17761909, https://doi.org/10.1161/STROKEAHA.107.490151.

Shirmohammadi F, Hasheminassab S, Saffari A, Schauer JJ, Delfino RJ, Sioutas C. 2016. Fine and ultrafine particulate organic carbon in the Los Angeles basin: trends in sources and composition. Sci Total Environ 541:1083–1096, PMID: 26473710, https://doi.org/10.1016/j.scitotenv.2015.09.133.

Shirmohammadi F, Sowlat MH, Hasheminassab S, Saffari A, Ban-Weiss G, Sioutas C. 2017. Emission rates of particle number, mass and black carbon by the Los Angeles International Airport (LAX) and its impact on air quality in Los Angeles. Atmos Environ 151:82–93, https://doi.org/10.1016/j.atmosenv.2016.12.005.

Squadrito F, Calapai G, Altavilla D, Cucinotta D, Zingarelli B, Campo GM, et al. 1994. Food deprivation increases brain nitric oxide synthase and depresses brain serotonin levels in rats. Neuropharmacology 33(1):83–86, PMID: 7514281, https://doi.org/10.1016/0028-3908(94)90100-7.

Sweeney MD, Montagne A, Sagare AP, Nation DA, Schneider LS, Chui HC, et al. 2019. Vascular dysfunction–the disregarded partner of Alzheimer's disease. Alzheimers Dement 15(1):158–167, PMID: 30642436, https://doi.org/10.1016/j.jalz.2018.07.222.

Taghvaee S, Mousavi A, Sowlat MH, Sioutas C. 2019. Development of a novel aerosol generation system for conducting inhalation exposures to ambient particulate matter (PM). Sci Total Environ 665:1035–1045, PMID: 30893735, https://doi.org/10.1016/j.scitotenv.2019.02.214.

Tonne C, Elbaz A, Beevers S, Singh-Manoux A. 2014. Traffic-related air pollution in relation to cognitive function in older adults. Epidemiology (Cambridge, Mass) 25:674–681, PMID: 25036434, https://doi.org/10.1097/EDE.0000000000000144.

Tsai TL, Lin YT, Hwang BF, Nakayama SF, Tsai CH, Sun XL, et al. 2019. Fine particulate matter is a potential determinant of Alzheimer's disease: a systemic review and meta-analysis. Environ Res 177:108638, PMID: 31421449, https://doi.org/10.1016/j.envres.2019.108638.

Turner MC, Cohen A, Jerrett M, Gapstur SM, Diver WR, Pope CA 3rd, et al. 2014. Interactions between cigarette smoking and fine particulate matter in the Risk of Lung Cancer Mortality in Cancer Prevention Study II. Am J Epidemiol 180(12):1145–1149, PMID: 25395026, https://doi.org/10.1093/aje/kwu275.

van Dalen JW, Mutsaerts H, Nederveen AJ, Vrenken H, Steenwijk MD, Caan MWA, et al. 2016. White matter hyperintensity volume and cerebral perfusion in older individuals with hypertension using arterial spin-labeling. AJNR Am J Neuroradiol 37(10):1824–1830, PMID: 27282862, https://doi.org/10.3174/ajnr.A4828.

Wakita H, Tomimoto H, Akiguchi I, Kimura J. 1994. Glial activation and white matter changes in the rat brain induced by chronic cerebral hypoperfusion: an immunohistochemical study. Acta Neuropathol 87(5):484–492, PMID: 8059601, https://doi.org/10.1007/BF00294175.

Wolters FJ, Zonneveld HI, Hofman A, van der Lugt A, Koudstaal PJ, Vernooij MW, et al. 2017. Cerebral perfusion and the risk of dementia: a population-based study. Circulation 136(8):719–728, PMID: 28588075, https://doi.org/10.1161/CIRCULATIONAHA.117.027448.

Woodward NC, Levine MC, Haghani A, Shirmohammadi F, Saffari A, Sioutas C, et al. 2017a. Toll-like receptor 4 in glial inflammatory responses to air pollution in vitro and in vivo. J Neuroinflammation 14(1):84, PMID: 28410596, https://doi.org/10.1186/s12974-017-0858-x.

Woodward NC, Pakbin P, Saffari A, Shirmohammadi F, Haghani A, Sioutas C, et al. 2017b. Traffic-related air pollution impact on mouse brain accelerates myelin and neuritic aging changes with specificity for CA1 neurons. Neurobiol Aging 53:48–58, PMID: 28212893, https://doi.org/10.1016/j.neurobiolaging.2017.01.007.

Younan D, Petkus AJ, Widaman KF, Wang X, Casanova R, Espeland MA, et al. 2020. Particulate matter and episodic memory decline mediated by early neuroanatomic biomarkers of Alzheimer's disease. Brain 143(1):289–302, PMID: 31746986, https://doi.org/10.1093/brain/awz348.

Zhang X, Kimura Y, Fang C, Zhou L, Sfyroera G, Lambris JD, et al. 2007. Regulation of toll-like receptor-mediated inflammatory response by complement in vivo. Blood 110(1):228–236, PMID: 17363730, https://doi.org/10.1182/blood-2006-12-063636.

Zhang Y, Schauer JJ, Shafer MM, Hannigan MP, Dutton SJ. 2008. Source apportionment of in vitro reactive oxygen species bioassay activity from atmospheric particulate matter. Environ Sci Technol 42(19):7502–7509, PMID: 18939593, https://doi.org/10.1021/es800126y.